Rare eclogite-mafic granulite in felsic granulite in Blanský les: precursor of intermediate granulite in the Bohemian Massif?

P. ŠTÍPSKÁ[1,2], R. POWELL[3], M. RACEK[4,5]

[1] *Center for Lithospheric Research, Czech Geological Survey, 11821 Praha 1, Czech Republic*

[2] *Ecole et Observatoire des Sciences de la Terre, Institut de Physique du Globe, CNRS UMR 7516, Université de Strasbourg, 1 rue Blessig, F-67084 Strasbourg Cedex, France*

[3] *School of Earth Sciences, University of Melbourne, Victoria 3010, Australia*

[4] *Institute of Petrology and Structural Geology, Charles University, 12843 Praha 2, Czech Republic*

[5] *Czech Geological Survey, 11821 Praha 1, Czech Republic*

ABSTRACT

Mafic granulite, generated from eclogite, occurs in felsic granulite at Kleť, Blanský les, in the Bohemian Massif. This is significant because such eclogite is very rare within the felsic granulite massifs. Moreover, at this locality, strong interaction has occurred between the mafic granulite and the adjacent felsic granulite producing intermediate granulite (see companion paper, Štípská *et al.*, this issue), such intermediate granulite being of enigmatic origin elsewhere. The mafic granulite involves garnet from the original eclogite, containing large idiomorphic inclusions of omphacite, plagioclase and quartz, as well as rutile. The edge of the garnet is replaced by a plagioclase corona, with the garnet zoned towards the corona and also the inclusions. The original omphacite-quartz-?plagioclase matrix has recrystallised to coarse-grained polygonal ("equilibrium"-textured) plagioclase-diopsidic clinopyroxene-orthopyroxene also with brown amphibole commonly in the vicinity of garnet. Somewhat-larger quartz grains are embedded in this matrix, along with minor ilmenite, rutile and zircon. Combining the core garnet composition with core inclusion compositions gives a pressure of the order of 18 kbar from assemblage and isopleths on a $P-T$ pseudosection, with temperature poorly constrained, but most likely greater than 900 °C. From this $P-T$ pseudosection, the recrystallisation of the matrix took place at about 12 kbar, and from Zr-in-rutile thermometry, at relatively hot conditions of 900–950 °C. It is largely at these conditions that the eclogite/mafic granulite interacted with the felsic granulite to make intermediate granulite (see next paper).

Key words: Bohemian Massif, eclogite, mafic granulite, Zr-in-rutile thermometry

INTRODUCTION

Eclogite, dominated by garnet and omphacitic clinopyroxene, and mafic granulite, dominated by garnet, omphacitic clinopyroxene and plagioclase are the most obvious expression of high pressure metamorphism when mafic compositions are metamorphosed under low $a(H_2O)$ (i.e. dry) conditions and/or high temperature (O'Brien & Rötzler, 2003; Rebay *et al.*, 2010; Liu *et al.*, 2011). The felsic granulite massifs of the Bohemian Massif are acknowledged to reflect metamorphic conditions of >850 °C, and, as they tend to contain kyanite and grossular-rich garnet, their pressure of formation is >16 kbar from thermobarometry (O'Brien & Rötzler, 2003) or on $P-T$ pseudosections (Racek *et al.*, 2006; Tajčmanová *et al.*, 2006; Štípská *et al.*, 2008; Franěk *et al.*, 2011a). At these $P-T$ conditions, mafic compositions will occur as eclogite or mafic granulite under dry conditions. However, eclogite and mafic granulite directly embedded in the felsic granulite massifs (not in peridotites) are rare (Medaris *et al.*, 1995b, 1998, 2006; Willner *et al.*, 2000; Rötzler & Romer, 2001; Štípská & Powell, 2005a). Rather it seems that the majority of pyroxene-bearing granulites are intermediate in composition, containing significant potassium, reflected petrologically in the presence of ternary feldspar and/or biotite (Fiala *et al.*, 1987; Carswell & O'Brien, 1993; Cooke, 2000; Cooke & O'Brien, 2001; O'Brien & Rötzler, 2003; Rötzler *et al.*, 2004; Štípská & Powell, 2005b; Sláma *et al.*, 2007; O'Brien, 2008; Racek *et al.*, 2008; Tajčmanová *et al.*, 2010).

At Kleť in the Blanský les massif (Fig. 1), such an eclogite-mafic granulite (referred to as eclogite below), in an unusually good state of preservation, occurs within intermediate granulite, adjacent to felsic granulite, in a low-strain zone. This eclogite is interesting in its own right as they are rare. However, its real significance lies in it being surviving material from the interaction between the eclogite and felsic granulite that has produced intermediate granulite. Given the excellence of the spatial context the formation of the intermediate granulite can be studied properly (see Štípská *et al.*, 2014, this issue). The characterisation of the eclogite needed for such a study is undertaken here, with, in particular, its $P-T$ path inferred from petrographic relations, Zr-in rutile thermometry and pseudosection modelling.

GEOLOGICAL SETTING

An overview of previous petrology of eclogite, felsic granulite and intermediate granulite is needed given that the eclogite described is considered as the surviving material from the interaction between eclogite and felsic granulite. This is presented following an outline of the overall geological context.

Tectonic setting of the Bohemian massif

The main tectonic domains of the Variscan Bohemian Massif are from the west to the east: the Saxothuringian, the Teplá-Barrandian, the Moldanubian and the Brunia domains (Fig. 1) (Schulmann *et al.*, 2009). The Saxothuringian continental and oceanic crust was partly subducted under the Teplá-Barrandian and Moldanubian continental domains in Devonian and Carboniferous times. The Moldanubian domain is considered to be the root of the orogen, (including the Orlica-Snieznik dome; e.g. Chopin *et al.*, 2012a). The majority of the Moldanubian high-grade rocks occurs in the Gföhl unit, composed mainly of kyanite−K-feldspar granulite (O'Brien & Rötzler, 2003) and the Gföhl orthogneiss (Hasalová *et al.*, 2008a, b, c), both hosting mafic to intermediate granulite and peridotite associated with eclogite and pyroxenite (e.g. Carswell, 1991; Medaris *et al.*, 1995b, 2005). At least part of the Gföhl unit is thought to be originally deeply subducted Saxothuringian crust (O'Brien, 2000; Janoušek & Holub, 2007; Lexa *et al.*, 2011; Nahodilová *et al.,* 2012). This origin is supported by the geochemical similarity of granulites with some Saxothuringian granites (Janoušek *et al.*, 2004), and their deep subduction is supported by finding of diamond and coesite in the Moldanubian granulites (Kotková *et al.*, 2011), and the presence of garnetiferous peridotites (Carswell, 1991). The rock association of kyanite−K-feldspar granulite, garnetiferous peridotite, eclogite, together with diamond-bearing quartzo-feldspathic rocks occurs also in the Saxothuringian domain (e.g. Stöckhert *et al.*, 2001; Schmädicke *et al.*, 1992, 2010; Willner *et al.,* 1997, 2000), pointing to a possible genetic link with the Moldanubian granulites. The granulites appear in NE-SW trending belts subparallel to the boundaries of the major tectonic domains (Fig. 1). This geometry is attributed to vertical exhumation of the lower crust to mid-crustal levels, where the rocks are reworked by shallow dipping structures (e.g. Willner *et al.*, 2000; Štípská *et al.*, 2004; Schulmann *et al.*, 2008; Jamieson *et al.*, 2011). Geochronology of the granulites and eclogites involves an extensive database of mainly zircon ages, clustering around 340 Ma, interpreted as the HP metamorphic climax (e.g. Kröner *et al.*, 2000). However, in detail, the meaning of zircon ages spreading from *c.* 500 Ma to *c.* 335 Ma is not yet fully understood (e.g. Bröcker *et al.*, 2010; Friedl *et al.*, 2011; Nahodilová *et al.*, 2012). Scarce garnet ages date the prograde metamorphic path (350 Ma, Sm−Nd method, Prince *et al.*, 2000; 387 Ma, Lu–Hf method, Anczkiewicz *et al.*, 2007).

Felsic granulites and Gföhl gneisses

The majority of felsic granulites are former granitoids, correlated with the Ordovician–Silurian meta-igneous rocks of the Saxothuringian domain (Janoušek *et al.*, 2004). Rarely

reported muscovite (*sensu lato*) in garnet suggests incipient eclogite facies conditions (Willner *et al.*, 1997; Faryad, 2009; Nahodilová *et al.*, 2012). The peak assemblage garnet-kyanite-ternary feldspars-quartz-rutile, has led to estimation of $P-T$ conditions in excess of 800°C and greater than 18 kbar (O'Brien, 2000; O'Brien & Rötzler, 2003, and references therein), and the discovery of coesite and microdiamond suggests subduction to UHP conditions (Kotková *et al.*, 2011). Decompression is commonly almost isothermal, into the sillimanite stability field (Tajčmanová *et al*., 2006; Štípská *et al*., 2010), in places is accompanied with significant cooling (Schulmann *et al.*, 2008). The Gföhl gneisses are Cambro–Ordovician granitoids (Schulmann *et al.*, 2005), locally metamorphosed under high-pressure conditions (Chopin *et al.*, 2012b, Cooke & O'Brien, 2001), in most places occurring as biotite migmatites, commonly with garnet and/or sillimanite (Hasalová *et al*., 2008c).

Eclogites and mafic granulites within felsic granulites and gneisses

Eclogite in the Gföhl granulite and gneiss has been classified by Medaris *et al.* (1995b) according to their surrounding rocks. These are either peridotites or serpentinites (group P), or felsic granulites or gneisses (group G). Eclogite is common in peridotite, interpreted as high-pressure crystal cumulates formed in the upper mantle (Medaris *et al.*, 1995a) or shallow Mg-rich cumulate gabbros transformed to eclogites (Obata *et al.*, 2006). The G type eclogite (Medaris *et al.*, 1995b; 1998; 2006; Štípská & Powell, 2005a) and the mafic granulite (Rötzler & Romer, 2001; Medaris *et al.*, 1998) are very rare in the Moldanubian domain, but are common in the Saxothuringian Erzgebirge (Schmädicke *et al.*, 1992; Klápová *et al.*, 1998) and the Orlica-Snieznik dome (Smulikowski, 1967). As the petrology of the individual eclogites and mafic granulites differs significantly, most likely reflecting different metamorphic histories, a petrographic description by occurrence is given below. More generalised ideas of their $P-T$ evolution, coming from phase equilibria are given in the Discussion. For more detail about the intermediate granulites, see Štípská *et al.* (2014).

The prograde character of eclogites in felsic granulite from the Moldanubian domain at Spačice and Jemnice localities (Medaris *et al.,* 1998, 2006; Štípská & Powell, 2005a), is based on prograde garnet profiles and inclusions within garnet that involve amphibole, epidote-group minerals, plagioclase and clinopyroxene (jd_{27}). Peak is inferred to occur in the garnet-omphacite (jd_{33})-rutile stability field and the coarse-grained recrystallized amphibole-diopside-plagioclase matrix without orthopyroxene indicates decompression in the amphibolite-facies conditions.

The *eclogites* associated with ky-ksp granulites in the Saxothuringian domain occur in the Gneiss-eclogite unit of the Central Erzgebirge (Schmädicke *et al.*, 1992). The peak assemblage comprises omphacite ($jd_{27–50}$), unzoned garnet, coesite, rutile, rare muscovite and kyanite. Retrogression involves limited growth of symplectite, amphibole, and replacement of muscovite by plagioclase and biotite.

The eclogites in the Orlica-Snieznik dome gneisses are most commonly composed of garnet and omphacite (jd_{36}), with variable accessory zoisite, muscovite, rutile, quartz and kyanite (Smulikowski, 1967; Bröcker & Klemd, 1996; Štípská *et al.*, 2012), with possible coesite (Bakun-Czubarow, 1991). The retrograde evolution involves fine-grained symplectite after omphacite and the development of an amphibolite facies assemblage of plagioclase, amphibole, biotite, ilmenite and sphene.

The mafic and intermediate granulites in the Orlica-Snieznik dome are intimately associated with each other. They are composed of omphacite (jd_{28}), garnet, plagioclase, quartz and rutile, in places with kyanite and/or mesoperthitic plagioclase (Pouba *et al.*, 1985; Steltenpohl *et al.*, 1993; Kryza *et al.*, 1996; Štípská *et al.*, 2004; Anczkiewicz *et al.*, 2007), with possible pseudomorphs after coesite (Klemd & Bröcker, 1999). Decompression involves growth of retrograde amphibole, in places also biotite or orthopyroxene.

The mafic granulite from the Saxonian granulite massif is composed of garnet, clinopyroxene, plagioclase, amphibole, titanite, spinel, magnetite and muscovite (Rötzler & Romer, 2001). Spinel and clinopyroxene ($jd_{2–3}$) is included in garnet. The peak metamorphic assemblage is inferred to involve the garnet core ($grs_{46–38}$), matrix clinopyroxene (jd_{10}) and titanite without quartz and plagioclase. The matrix is recrystallized to clinopyroxene-plagioclase-magnetite with amphibole.

The Spačice pyroxene granulite from the Moldanubian zone is composed of garnet, clinopyroxene, plagioclase, quartz, rutile, ilmenite and amphibole (Medaris *et al.*, 1998). Garnet includes amphibole and shows decreasing spessartine and grossular ($sps_{7=>0}$, $grs_{32=>25}$), interpreted as prograde features. The matrix is recrystallized into coarse-grained symplectite of clinopyroxene (jd_{10}) and plagioclase with some retrograde amphibole.

PETROGRAPHY AND MINERAL CHEMISTRY

Analytical procedures and abbreviations

The whole rock ICP-MS analyses were performed in the Acme laboratories, Canada. Mineral analyses were obtained on an electron microprobe CAMECA SX-100 at the Institute of

Mineralogy at the University of Stuttgart in point beam mode at 15 kV and 15 nA and on a scanning electron microscope Tescan VEGA with X-Max 50 EDS detector at the Institute of Petrology and Structural Geology at the Faculty of Science of the Charles University in Prague in point beam mode at 15 kV and 1.5 nA.

The field relations are shown in Fig. 2, the petrography is documented in Figs 3,4 & 5, representative mineral analyses are summarized in Tables 1−3, garnet, plagioclase, clinopyroxene and amphibole chemistry are shown in Figs 6 & 7. Rutile was analysed for Si and Nb to screen for the possibility of micro-inclusions of zircon and the zirconium in rutile thermometry is portrayed in Fig. 8. The sign "=>" is used for a trend in mineral composition or for zoning and the sign "–" for a range of mineral compositions; p.f.u. = per formula unit (pyroxene recalculated on 6 oxygens, garnet 12, feldspar 8, and amphibole 23 oxygens and cations 13+Na+Ca+K).

Mineral abbreviations: g = garnet, cpx = clinopyroxene, o = omphacitic clinopyroxene, jd = jadeitic clinopyroxene, di = diopsidic clinopyroxene, opx = orthopyroxene, am = amphibole, hb = hornblende, pl = plagioclase, q = quartz, ilm = ilmenite, ru = rutile, mt = magnetite, zrc = zircon; alm = $Fe^{2+}/(Ca + Fe^{2+} + Mg + Mn)$, py = $Mg/(Ca + Fe^{2+} + Mg + Mn)$, grs = $Ca/(Ca + Fe^{2+} + Mg + Mn)$, sps = $Mn/(Ca + Fe^{2+} + Mg + Mn)$, XFe = $Fe^{2+}/(Fe^{2+} + Mg)$, an = Ca/(Ca + Na + K), ab = Na/(Ca + Na + K), jd = Na/(Na + Ca). Ferric iron is estimated by charge-balance. The isopleth notation used is: (z(g) = $Ca/(Ca + Fe^{2+}+ Mg)*100$, j(cpx) = Na/(Na + Ca)*100, ca(pl) = Na/(Na + Ca)*100.

Petrography

Eclogite samples were collected at the Kleť mountain, in a low strain domain of felsic granulite in the core of the Blanský les massif (Franěk *et al.*, 2006; 2011a,b). The eclogite occurs as centimetre- to metre-scale oval-shaped bodies within intermediate granulite, at an outcrop dominated by intermediate granulite with subordinate felsic granulite (Fig. 2a,b). The eclogite grades into the intermediate granulite which abuts the felsic granulite. The formation of the intermediate granulite is the subject of the companion paper (Štípská *et al.,* 2014). Macroscopically, the eclogite has a greenish fine-grained matrix with variable proportions of fine-grained amphibole-rich black domains and millimetre-size red garnet (Fig. 2c−f). 20 thin sections were studied from one large piece of the eclogite, sampled within an oval-shaped body 0.5m size across. Two whole rock ICP-MS analyses were obtained from the core and from the rim of the same body, respectively (in wt%, sample KL1i: SiO_2 = 51.51, Al_2O_3 = 15.41, MnO = 0.16, CaO = 9.64, MgO = 8.47, Fe_2O_3 = 10.84, Na_2O = 3.05, K_2O = 0.12, TiO_2

198 = 1.20, P_2O_5 = 0.12, Cr_2O_3 = 0.06; FeO analyzed = 8.65, so by difference 11.34% of Fe is
199 present as Fe^{3+}; sample KL2R1: SiO_2 = 51.03, Al_2O_3 = 14.87, MnO = 0.16, CaO = 9.56, MgO
200 = 8.24, Fe_2O_3 = 11.02, Na_2O = 2.87, K_2O = 0.20, TiO_2 = 1.27, P_2O_5 = 0.09, Cr_2O_3 = 0.05; FeO
201 analyzed = 9.25, so by difference 6.74% of Fe is present as Fe^{3+}).
202 As shown by BSE imaging, as well as under the microscope, the matrix has a coarse-
203 grained (50−150μm), equilibrated microstructure with straight grain boundaries and triple
204 junctions between grains (Fig. 3a,b). It is formed of diopsidic clinopyroxene, orthopyroxene,
205 plagioclase and quartz, which constitute 60−70% of the rock. Quartz has rare contacts with
206 plagioclase and tends to be surrounded by diopsidic clinopyroxene and orthopyroxene (Fig.
207 3a,b,f). Brown amphibole (5−20%, 50−150 μm) tends to occur within this coarse-grained
208 matrix in the vicinity of garnet (Figs 3f & 6). The modal content of garnet is 10−25%. Garnet
209 contains large inclusions of omphacite (up to 500 μm in size), plagioclase (up to 50 μm in
210 size) and quartz (up to 50 μm in size) that tend to have idiomorphic shapes (Fig. 4). Garnet is
211 surrounded by a multi-grained corona of plagioclase (Fig. 3c,f). Within the corona, garnet
212 may be embayed by kelyphite composed of plagioclase and green amphibole, locally with
213 small orthopyroxene (20 μm) and ilmenite. Accessory minerals are zircon, rutile, ilmenite and
214 apatite. Rutile and zircon occur included in garnet and in the matrix. Ilmenite occurs as
215 lamellae in some rutile. Proportions of garnet, garnet with kelyphite and garnet with kelyphite
216 and plagioclase corona were calculated for the whole thin section KL2N and separately for a
217 garnet-rich area within the same thin section (Fig. 5). The proportions are 11% and 25%, 17%
218 and 31%, and 33% and 43%, respectively.

219 **Mineral chemistry**

220 The garnet has a compositionally flat core ($grs_{0.22\text{-}0.26}\,alm_{0.30\text{-}0.36}\,py_{0.32\text{-}0.36}\,sps_{0.01}$, XFe =
221 0.50−0.52) and shows decrease of grossular and pyrope, with simultaneous increase of
222 almandine and XFe, at the rim (for example to $grs_{0.15}\,alm_{0.50}\,py_{0.30}\,sps_{0.02}$, XFe = 0.63) (Fig.
223 7a). The decrease of grossular occurs at the contact with the plagioclase corona, but less so at
224 the contact with the kelyphite (Fig. 6). Garnet is also zoned around inclusions. Clinopyroxene
225 included in garnet is omphacite with a flat compositional profile in the core (jd = 0.40−0.43,
226 Ca = 0.47−0.50 p.f.u., Al^{IV} = 0.06 p.f.u., XFe = 0.21), and a rim marked by decrease in jadeite
227 and XFe and increase in diopside and Al^{IV} (jd = 0.22, Ca = 0.68 p.f.u., Al^{IV} = 0.15 p.f.u., XFe
228 = 0.18; Fig. 7c). Next to these omphacite inclusions, grossular decreases, and pyrope and
229 almandine increases significantly ($grs_{0.18}\,alm_{0.41}\,py_{0.40}\,sps_{0.01}$, XFe = 0.50) (Fig. 7a). In
230 contrast to the inclusions in garnet, matrix clinopyroxene is diopsidic (jd = 0.01−0.07, Ca =

231 0.85−0.90 p.f.u., Al^{IV} = 0.03−0.10 p.f.u., XFe = 0.20; Fig. 7c). Orthopyroxene has Al^{IV} =
232 0.03−0.05, XFe = 0.36 and Ca = 0.02−0.03 p.f.u.
233 Plagioclase composition varies according to its textural position (Fig. 7b). Inclusions
234 in garnet have the composition of around $an_{0.27}$–ab_{73}–$or_{0.01}$. Matrix plagioclase is zoned with
235 increase of anorthite from core to rim ($an_{0.29}$–$ab_{0.70}$–$or_{0.01}$ => $an_{0.40}$–$ab_{0.60}$–$or_{0.00}$). Plagioclase
236 grains making up the corona around garnet show similar zoning to grains in the matrix (Fig.
237 6), with a tendency towards asymmetric profiles showing a greater increase of anorthite next
238 to garnet (up to $an_{0.70}$–$ab_{0.30}$–$or_{0.00}$) than next to matrix clinopyroxene or orthopyroxene
239 ($an_{0.32–0.47}$–$ab_{0.68–0.53}$–$or_{0.01}$; Fig. 6). Plagioclase within the kelyphite has up to 90% of
240 anorthite ($an_{0.55–0.90}$–$ab_{0.45–0.10}$–$or_{0.00–0.01}$).
241 Amphibole is pargasitic and shows slightly different composition for the brown matrix
242 grains (in p.f.u.: Si = 6.32−6.45, Al^{IV} = 0.26−0.32, Na(A) = 0.38−0.41, Na(M4) = 0.10−0.14,
243 K = 0.19−0.20, Ti = 0.23−0.36; XFe = 0.26−0.37) and green grains in the kelyphite (in p.f.u.:
244 Si = 6.15−6.27, Al^{IV} = 0.40−0.48, Na(A) = 0.28−0.35, Na(M4) = 0.14−0.20, K = 0.15−0.22,
245 Ti = 0.07−0.12; XFe = 0.17−0.29). The major difference is in the greater Ti, and also Si,
246 Na(A), and XFe, and the lesser Al^{VI} in the matrix amphibole compared to the kelyphite.

247 **Zr in rutile**

248 The Zr content of rutile was used to calculate the temperature according to Tomkins *et al.*
249 (2007). This thermometer includes a pressure dependence for the substitution of Zr in rutile
250 coexisting with zircon and quartz. Box-plots of the Zr content and calculated temperatures are
251 shown in Fig. 8, at 18 kbar for rutile included in garnet, and at 12 kbar for various textural
252 settings of matrix rutile. Zr contents in rutile show ranges of: 1000−2500 ppm for rutile
253 included in garnet, 3000−4500 ppm for the matrix rutile with or without ilmenite lamellae,
254 and 4500−7000 ppm for rutile that seems to be intimately associated with ilmenite. The upper
255 temperature ends of the boxes are used to indicate a representative temperature for each
256 textural context giving 900 °C, 950 °C, and 1000 °C, respectively, following the suggestion of
257 Tomkins *et al.* (2007). Given that the temperatures obtained may be too high or too low if a
258 rutile was not in communication with quartz or zircon when it grew, a conservative estimate
259 of temperature of equilibration of the matrix is 950 °C, as discussed below.

PSEUDOSECTION MODELLING

Calculation methods and strategy

The pseudosections were calculated using THERMOCALC 3.3 (Powell *et al.*, 1998, 2009 version) with dataset 5.5 (Holland & Powell, 1998, November 2003 upgrade), in the system Na_2O-CaO-FeO-MgO-Al_2O_3-SiO_2-H_2O-TiO_2-O (NCFMASHTO) with the amphibole model of Diener *et al.* (2007) modified by Diener & Powell (2012), clinopyroxene from Green *et al.* (2007) modified by Diener & Powell (2012), garnet from White *et al.* (2007) modified by Powell (unpubl., 2008) and used in all following work, and orthopyroxene from White *et al.* (2007), feldspar from Holland & Powell (2003), and ilmenite from White *et al.* (2000). There are two main ways that the available models do not correspond to the observed mineral compositions: the clinopyroxene model does not include the cats end-member (up to a proportion of 0.1 in the matrix clinopyroxene and up to 0.15 in the omphacite inclusion rim), and the amphibole model does not include K or Ti (of the order of 0.2 p.f.u. and 0.3 p.f.u. respectively in the matrix amphibole). In addition there is no current melt model for mafic compositions. It is unlikely that the cats substitution at this level will dramatically affect the phase relationships, but might be more significant to higher temperatures than those of interest here. However it is possible that this shortcoming will affect the calculated jadeite contents of clinopyroxene, particularly at lower pressures. K and Ti in amphibole will have the effect of stabilising amphibole, but the main calculations do not involve H_2O or amphibole, because of the absence of an appropriate melt model. Petrographic observation suggests that the eclogite was unlikely to have melted, so this absence only relates to a negative constraint on conditions of formation.

For the pseudosections, the whole rock ICP-MS analyses were used. The Fe_2O_3 was set to be 9% of the total FeO, very close to the average of the two analysed samples (9.04%), and corresponding to the mean value obtained for ocean floor basalts (Sun & McDonough, 1989; Rebay *et al.*, 2010).

The pseudosection in NCFMASTO (ie "dry") is calculated to discuss peak $P-T$ conditions and the retrograde path of the anhydrous eclogite assemblage (Fig. 9). The approximate effect of some garnet proportion not being part of the effective whole rock composition during decompression is examined using a $P-X$ diagram (Fig. 10). Such a dry pseudosection obviously cannot be used to consider the small amount of amphibole observed in the equilibrated matrix. Additionally, later replacement of garnet by plagioclase-amphibole kelyphite cannot be considered. However in the absence of a melt model for mafic rocks, the

role of H_2O cannot be studied properly. However it is still worth trying to explore the effect of H_2O on phase relations, even though this is at best approximate for the appearance of melt, and acknowledging the possibility that the stabilising effect of K and Ti is responsible for the observed amphibole in the matrix. This is done using a $P-T$ pseudosection (Fig. 11), and with $T-M(H_2O)$ and $T-\mu(H_2O)$ diagrams (Fig. 12).

Dry *P*−*T* pseudosection

A dry pseudosection (Fig. 9) is calculated for the composition of the eclogite sample KL1i. The pseudosection shows fields of mineral assemblages stable at eclogite and granulite facies conditions and is contoured with the calculated molar proportion isopleths for garnet and compositional isopleths for garnet, clinopyroxene and plagioclase.

The mineral assemblage in the eclogite was garnet, omphacite, quartz and rutile. Plagioclase is included in some garnets, in the vicinity of omphacite inclusions. It is therefore likely that at least part of garnet crystallized in the presence of both omphacite and plagioclase, which corresponds in the pseudosection to the g-cpx-pl-ru-q field. However, it is not excluded that part of garnet crystallization occurred outside the stability of plagioclase. Garnet core compositions (grs = 0.23−0.27) and clinopyroxene core compositions in the inclusions (jd = 0.40−0.43) are consistent with the calculated isopleths in the higher pressure part of the g-cpx-pl-ru-q field. The predicted molar proportion of garnet between 40 and 45 mol. % at these conditions suggests that both the plagioclase corona and kelyphite developed at the expense of garnet and not only around it. Compositions at the rim of the clinopyroxene inclusions (jd = 0.25), garnet next to them (grs = 0.15), and the chemistry of the included plagioclase (an = 0.27) point to reequilibration of these contacts accompanying decompression.

The texturally-equilibrated matrix dominated by clinopyroxene, orthopyroxene and plagioclase points to decompression into the g-cpx-opx-pl-ru-q field. The garnet rim composition next to plagioclase (grs = 0.12−0.18) and matrix plagioclase composition ($an_{0.30->0.40}$) fit closely the calculated isopleths in this field. However the jadeite content of the matrix clinopyroxene (jd = 0.07) is much lower than the calculated isopleths. The unaccounted-for cats end-member in the matrix clinopyroxene (Al^{IV} = 0.04−0.10) may be responsible for the discrepancy. The predicted molar proportion of garnet (in the range 15−30 mol. %) corresponds to the observed proportion of garnet if combined with the plagioclase corona estimated from the thin section (Fig. 5). This suggests that a substantial proportion of the

garnet was replaced by plagioclase, rather than the plagioclase growing on the garnet (e.g. as plagioclase grows on kyanite, not replacing it, e.g. Štípská *et al.*, 2010).

The microstructural evolution and mineral chemistry therefore record decompression from eclogite (or highest-pressure granulite) conditions to medium-pressure granulite conditions. The temperature from Zr-in-rutile thermometry indicates 900˚C (at 18 kbar) for rutile included in garnet and 950˚C (at 12 kbar) for matrix rutile (Fig. 8). It is likely that the equilibration of the matrix therefore occurred at very high temperature, of the order of 950˚C, at a pressure around 12.5 kbar. It has not been established why temperatures from Zr-in-rutile thermometry from rutile inclusions in garnet are somewhat lower.

Dry *T*−*X* pseudosection with variable proportion of garnet

The effect of the interior part of the garnet not being part of the effective bulk composition controlling the matrix phase relationships is discussed with the aid of a *P*−*X* diagram (Fig. 10). The *X* axis represents variation from the original whole rock composition of the sample KL1i to the whole rock composition KL1i with all garnet subtracted, at 20 kbar and 950 ˚C (from 0 to 1 on the *X* axis). Such an approach is necessarily approximate as the breakdown of communication of the interior part of the garnet with the matrix during decompression is a chemical potential effect not readily handled by an effective bulk composition approach. The zoned plagioclase corona reflects the fact that it grew under the action of chemical potential gradients (e. g. Štípská *et al.*, 2010).

The main impact on overall phase equilibria is that orthopyroxene appears at higher pressure with decompression, followed by garnet disappearing at higher pressure, if an increasing proportion of garnet is not part of the equilibration volume. The effects are discussed in terms of three types of paths on the diagram, labeled A, B and C. For path A, almost all garnet is in equilibrium on decompression and the path ends at 12.5 kbar with 10−15 mol. % garnet, around 15 % of grossular in garnet and 40−45 % of anorthite in plagioclase. This is not credible for the rock studied, because the garnet cores still show compositions corresponding to high pressure equilibration. Moreover there would be no reasonable explanation for the presence of the plagioclase corona, which presumably reflects reaction between the garnet and the matrix to decrease garnet mode.

For path B, only a small part of the garnet is in equilibrium with matrix, and the path ends in the garnet-absent cpx-opx-pl-ru-q field. Given that garnet is observed in the rock, this is not a possible scenario. It would imply that the garnet is efficiently reacted out of the rock and the rock would become garnet-absent at about 17 kbar.

For path C, only a small part of the garnet is in equilibrium with the matrix, and as garnet mode wants to decrease on decompression, the necessary proportion of garnet is consumed (for example via the growth of the plagioclase corona) and another small proportion of garnet becomes part of the matrix equilibration volume. Therefore the path is oblique on the diagram and ends at 12.5 kbar with the same amount of garnet and the same mineral compositions as path A. Because the garnet cores in the sample studied preserve their composition from high pressure and therefore are still isolated from the matrix, the path C is the more likely scenario for the behavior of the rock studied. On decompression, the garnet rim is in equilibrium with the matrix, changes therefore its composition, and simultaneously is progressively consumed (by the plagioclase corona, with Na coming from the matrix, and Fe and Mg added to the matrix). As it is consumed, the new outermost part of garnet becomes the rim, starts to be in equilibrium with the matrix and is consumed. Then the rock ends as observed, with 10−15% of garnet, isolated garnet cores with composition corresponding to high pressure equilibration, garnet rim compositions with 11−16% of grossular, and plagioclase rim compositions with around 40−45% of anorthite, which fits approximately the mineral assemblage and calculated isopleths at around 12.5 kbar.

Because the compositional isopleths of grossular and anorthite are subhorizontal on the diagram in the g-cpx-opx-pl-ru-q field corresponding to the observed matrix mineral assemblage, the equilibration mineral chemistry is similar whether all garnet or up to half of the garnet is part of the equilibration volume. The resulting equilibration at medium pressure therefore may be discussed directly in the dry $P-T$ pseudosection.

H_2O-undersaturated pseudosection

The effect of minor H_2O on phase equilibria is studied in an H_2O-undersaturated pseudosection (Fig. 11). The position of the [H_2O] line is critically dependent on the mole % H_2O chosen for the calculations (here, 0.2 %). As the amount is decreased, the line moves up pressure, converging on the position of [hb] which is independent of the mole % H_2O. Given that melting is precluded by the absence of a melt model for mafic rocks, the high temperature part of the pseudosection is likely to be metastable with respect to melt. The solidus is likely to be sub-parallel to [H_2O], and [liq] (if we could calculate it) would occur down pressure from [H_2O], but probably not by a lot (<50 °C), and the corresponding [hb] would be close to it. These relationships can be thought of in terms of the $a(H_2O)$ being less than 1 for melting, but $a(H_2O) = 1$ for H_2O-present.

Given that the amphibole model does not include K and Ti, the position of both [H_2O] and [hb] will be displaced up pressure (amphibole is stabilised) with respect to those calculated for a given mole % H_2O. Analogously both [liq] and its [hb] will be displaced up pressure. So, on balance the phase relationships in Fig. 11 might be close to correct, with the effect of melting counteracting that of the unaccounted-for solid solution in amphibole. In Fig. 11, the H_2O-bearing fields should instead be considered to be melt-bearing. A small amount of melt will not influence the solid phase equilibria above the solidus significantly. Amphibole is stable below the solidus, and its presence will not significantly influence the stability of the g-cpx-opx-pl-ru-q field compared to the dry pseudosection, nor if K and Ti could be considered. At least in part this is because the molar proportion of amphibole is essentially constant below the solidus, controlled by the mol. % H_2O in the bulk composition. If Fig. 11, but with H_2O replaced by liq in the labelling, is considered to be correct, then this may account for the small amount of hornblende occurring in the equilibrated hbl-cpx-opx-pl matrix.

$T-M(H_2O)$ and $T-\mu(H_2O)$ diagram

The microstructural observations suggest that the coarse-grained equilibrated matrix of clinopyroxene-orthopyroxene-plagioclase involving also 5−10% of brown hornblende was developed first, and that the plagioclase corona around garnet had developed by this time, most likely while decompression proceeded. Then, within the plagioclase corona, garnet is invaded by fine-grained green amphibole-plagioclase kelyphite in the form of embayments, suggesting that the fine-grained kelyphite developed later than the coarse-grained matrix. This sequence of microstructural development is also supported by the style of garnet zoning next to the plagioclase corona and next to kelyphite, with, respectively, a smooth grossular decrease to the edge of the garnet, and the kelyphite growth cutting across pre-existing zoning, with only a minor response in the garnet (grossular decrease). This will have occurred to lower temperature, when diffusion was less effective. Kelyphite growth cannot be explained in the H_2O-undersaturated $P-T$ pseudosection, because its development requires an additional amount of H_2O fluxed/diffused into the rock on cooling. Therefore, $T-M(H_2O)$ and $T-\mu(H_2O)$ diagram were constructed (Fig. 12). The first diagram allows consideration of the addition of H_2O without attention to process, whereas the second allows the likely method of access of the H_2O to be considered: diffusion.

In the $T-M(H_2O)$ the x axis ranges from the dry composition of the eclogite to a composition that allows H_2O-saturated assemblages (with H_2O in the bulk ranging from 0 to 5

mol %, unnormalised; Fig. 12a). With orthopyroxene still present in the rock only paths in the g-cpx-opx-pl-hb-ru-q field are of interest. In this field the hornblende mole proportion contours are vertical as amphibole is the only resident for the H_2O. Two paths, labelled A and B are discussed. Along path A, the limited amount of H_2O allows less than 5 mol. % of hornblende to be stable. This would appear in a rock as a single generation of hornblende, for example accounting for the matrix brown hornblende, but not the kelyphite growth. Along path B, more H_2O allows around 10 mol% of hornblende to form at higher temperature. In order to make more hornblende, it is necessary to increase the amount of H_2O in the bulk (horizontal arrow, Fig. 12a). Such a path will result in two generations of amphibole, the one crystallized at higher temperature, and the other at lower temperature (at the *T* of the horizontal arrow). This is the likely case for the rock studied, as it accounts for the first generation of brown amphibole in the coarse grained matrix, and the later development of the fine-grained green amphibole in the kelyphite replacing garnet. As in the discussion of Fig. 11 above, the effect of considering melt, combined with the counteracting effect of shortcomings in the amphibole model, means that the current figure can be considered with H_2O replaced with liq.

If diffusion is the process involved in adding H_2O to the rock to allow kelyphite growth, then the appropriate phase diagram should have $\mu(H_2O)$ on an axis (Fig. 12b). The $T-\mu(H_2O)$ diagram has the same topology as the $T-M(H_2O)$ diagram, with the [H_2O] line there corresponding to the edge of the inaccessible area here (Fig. 12). Now the amphibole mode contours are oblique. The same paths A and B are plotted. Path A, follows the 5 mol. % amphibole isopleth and this can be thought of as an internal buffering path. For path B, the path follows the 10 mol. % isopleth for amphibole. In order to increase the amount of amphibole to form the kelyphite, an increase in $\mu(H_2O)$ is needed. This should be thought of as the result of a superimposed $\mu(H_2O)$ from the surrounding rocks, e.g. felsic granulites or partial melts from the felsic granulites. This external $\mu(H_2O)$ pulls the path across (horizontal arrow) towards the value superimposed by the environment of the rock. Considering the presence of melt, this will form a narrow band (of unknown width) towards the $+H_2O$ line.

The H_2O addition to make the kelyphite may happen by H_2O influx or by diffusion. In the case of influx into the vicinity of the kelyphite, the H_2O would be incorporated into the kelyphite, but only if sufficient H_2O is added will the vicinity become H_2O-saturated. We can observe from the phase equilibria that H_2O-saturation would generate a large proportion of hornblende (>50%) rather than the 10% observed. Much more likely is that the vicinity will

be H_2O undersaturated, with the proportion of amphibole simply corresponding to the H_2O added. Regardless there will be a $\mu(H_2O)$ gradient set up away from where the H_2O is added. More distal addition of H_2O will set up such a $\mu(H_2O)$ gradient, and analogously an adjacent rock with greater $\mu(H_2O)$ will set up a gradient, both superimposing their $\mu(H_2O)$ on the garnet rim, with the capacity of growing the kelyphite.

DISCUSSION AND CONCLUSIONS

We have established the $P-T$ and corresponding textural evolution in this eclogite, as summarised in Fig. 13: 1) equilibration of high grossular garnet core and omphacite inclusions (in places with plagioclase) at 18−20 kbar; 2) decompression to 12 kbar at 950 °C, with decompression accompanied by the growth of the plagioclase corona; 3) recrystallisation of the matrix to texturally-equilibrated diopsidic clinopyroxene-orthopyroxene-plagioclase-brown amphibole with surviving garnet following decompression; 4) development of the zoning at plagioclase contacts; and 5) development of the kelyphitic replacement of garnet.

Regarding the Zr-in-rutile thermometry used to constrain the temperature of equilibration of the matrix at 950 °C, it is suggested that the rutile with ilmenite involved textural modification in the absence of communication with quartz, so the calculated temperatures above 950 °C for such rutile do not reflect formation conditions. It is feasible that the rutile in garnet had lost contact with zircon following envelopment, and there followed a redistribution of Zr between rutile and garnet on cooling. Thus their temperatures also do not reflect formation conditions. Alternatively the rutile and the enclosing garnet could have crystallised at the lower temperature.

The high temperature of the reworking of the eclogite at 12 kbar is interesting on several counts. The first relates to the observed survival of garnet with a high-pressure character (e.g. high grossular), indicating that the interior part of the garnet was essentially isolated from the matrix while the matrix was profoundly recrystallised, at the high temperature of 950 °C. The zoning in the garnet and the consumption of the garnet rim by the plagioclase corona is consistent with this idea of isolation. While the zoning in the plagioclase corona has been modified by re-equilibration during cooling around all plagioclase grains in the corona and the matrix, a plausible interpretation is that, before this modification took place, the zoning across the corona was strongly asymmetric, as expected in a diffusion-controlled situation.

The commonly adopted view would be that sluggish kinetics, with evidence of chemical potential gradients essentially preserved, is responsible for what is observed as a

consequence of the decompression. The big question is whether the diffusion coefficients combined with the likely time that the decompression took are consistent. The diffusion coefficients are not very well known, but the implication is that there cannot be consistency (e.g. Tajčmanová *et al.*, 2014). It might be noted that the high temperatures given by the Zr-in-rutile thermometer raise serious questions themselves because they are much higher than expected from closure temperature arguments (Watson *et al.*, 2006; Racek *et al.*, 2008; Kooijman *et al.*, 2012). The decompression is likely to be fast given the ubiquity of 340 Ma ages in the Bohemian Massif, but not fast enough to correspond to the rutile diffusion data (Fig. 9 in Racek *et al.*, 2008). An alternative, developed in Tajčmanová *et al.* (2014), is that grain-scale pressure variations occur, which for the rocks considered here would involve the central part of the garnet being still at elevated pressure while the matrix was recrystallising at 12 kbar. The zoned plagioclase corona would then be part of a pressure variation at diffusive equilibrium (see Tajčmanová *et al.*, 2014).

Comparing the Kleť eclogite with other mafic rocks reported from the granulites and Gföhl type orthogneisses we underline the remarkable scarcity of eclogites and mafic granulites within the felsic granulite bodies (Fiala *et al.*, 1987). Some show prograde features and retrogression under amphibolite facies, in which way they differ from the Kleť eclogite (Medaris *et al.*, 1998, 2006; Štípská & Powell, 2005a; Faryad, 2009; Štípská *et al.*, 2012). The coesite-bearing eclogites from the Gneiss-eclogite unit from the Central Erzgebirge in the Saxothuringian zone show equilibration at UHP conditions and retrogression at amphibolite-facies conditions (Schmädicke *et al.*, 1992). The only mafic granulites with low potassium, and therefore being without ternary feldspar, K-feldspar, or biotite, are described from the Saxonian granulite massif (Rötzler & Romer, 2001) and Spačice granulite (Medaris *et al.*, 1998). The granulites described from the Orlica-Snieznik dome are both mafic and intermediate types, and the features of the intermediate types are discussed in Štípská *et al.* (2014). Each of these occurrences differs from the Kleť mafic granulite. It seems that even if the Spačice granulite preserves prograde garnet zoning, the clinopyroxene (jd_{10}) is reequilibrated at medium pressure. The clinopyroxene with 10 % of jadeite in the Saxonian granulite seems also to have reequilibrated at medium pressure, and the clinopyroxene with 2% of jadeite included in garnet, and associated with spinel cannot be interpreted as equilibrated at high pressure. In such circumstances, even if garnet compositions are interpreted to be preserved from high pressure, they cannot be combined with matrix clinopyroxene to derive the peak $P-T$ conditions at high-pressure. In contrast, the Kleť eclogite preserves clinopyroxene inclusions with high jadeite content (up to 43 %) in garnet

with high grossular content (25−27 %), so with compositions that are compatible with predicted eclogite-facies mineral compositions. The presence of plagioclase in the same garnet, in places included with omphacite, is consistent with the rock being at some point equilibrated at the transition of eclogite and high-pressure granulite conditions. The petrographic features associated with decompression, involving the plagioclase corona replacing garnet, reequilibration of garnet rim to lower grossular compositions, recrystallization of matrix to coarse aggregate of clinopyroxene, orthopyroxene and plagioclase with some amphibole, and late replacement of garnet by plagioclase-amphibole dominated kelyphite is consistent with the major reequilibration features from the Saxonian or Spačice mafic granulites.

A further aspect of the high temperature at 12 kbar concerns the behaviour of the orogen if such high temperatures are regional in the orogenic root. In the context of the gravitational/convective inversion of the less dense orogenic root (Lexa *et al.*, 2011), it is not clear whether it could heat up areally to such a temperature without inverting. Thus, were the rocks studied here locally hot, e.g. associated with the intrusion of mafics or incorporation of ultramafic/mafic complexes into the orogenic root, but that areally most of the orogenic root was cooler?

ACKNOWLEDGEMENTS

We gratefully acknowledge the financial support of the Czech National Grant Agency (13-16315S to P. Štípská and O. Lexa), the Ministry of Education of the Czech Republic (grant LK11202 to K. Schulmann), the French National Grant Agency (ANR DSP-Tibet). RP acknowledges ARC DP0987731. T. Theye from the Institute of Mineralogy at the University of Stuttgart is thanked for operating the microprobe. Two anonymous reviewers are thanked for their constructive reviews, and D. Robinson is thanked for his editorial work.

548 **References**

549 Anczkiewicz, R., Szczepanski, J., Mazur, S., Storey, C., Crowley, Q., Villa, I. M., Thirlwall,
550 M. E. & Jeffries, T. E., 2007. Lu-Hf geochronology and trace element distribution in
551 garnet: Implications for uplift and exhumation of ultra-high pressure granulites in the
552 Sudetes, SW Poland. *Lithos*, **95**, 363–380.
553 Bakun-Czubarow, N., 1991. On the possibility of occurence of quartz pseudomorph after
554 coesite in the eclogite-granulite rock series of the Zlote Mountains in the Sudetes (SW
555 Poland). *Archiwum Mineralogiczne*, **47**, 5–16.
556 Bröcker, M. & Klemd, R., 1996. Ultrahigh-pressure metamorphism in the Snieznik Mountains
557 (Sudetes, Poland): P-T constraints and geological implications. *Journal of Geology*,
558 **104**, 417–433.
559 Bröcker, M., Klemd, R., Kooijman, E., Berndt, J. & Larionov, A., 2010. Zircon
560 geochronology and trace element characteristics of eclogites and granulites from the
561 Orlica-Snieznik complex, Bohemian Massif. *Geological Magazine*, **147**, 339–362.
562 Carswell, D. A., 1991. Variscan high P-T metamorphism and uplift history in the
563 Moldanubian Zone of the Bohemian Massif in Lower Austria. *European Journal of*
564 *Mineralogy*, **3**, 323–342.
565 Carswell, D. A. & O´Brien, P. J., 1993. Thermobarometry and geotectonic significance of
566 high-pressure granulites: Examples from the Moldanubian Zone of the Bohemian
567 Massif in Lower Austria. *Journal of Petrology*, **34**, 427–459.
568 Chopin, F., Schulmann, K., Skrzypek, E., Lehmann, J., Dujardin, J. R., Martelat, J. E., Lexa,
569 O., Corsini, M., Edel, J. B., Štípská, P. & Pitra, P., 2012a. Crustal influx, indentation,
570 ductile thinning and gravity redistribution in a continental wedge: Building a
571 Moldanubian mantled gneiss dome with underthrust Saxothuringian material
572 (European Variscan belt). *Tectonics*, **31**, TC1013.
573 Chopin, F., Schulmann, K., Štípská, P., Martelat, J. E., Pitra, P., Lexa, O. & Petri, B., 2012b.
574 Microstructural and metamorphic evolution of a high-pressure granitic orthogneiss
575 during continental subduction (Orlica-Snieznik dome, Bohemian Massif). *Journal of*
576 *Metamorphic Geology*, **30**, 347–376.
577 Cooke, R. A., 2000. High-pressure/temperature metamorphism in the St. Leonhard Granulite
578 Massif, Austria: evidence from intermediate pyroxene-bearing granulites.
579 *International Journal of Earth Sciences*, **89**, 631–651.

580 Cooke, R. A. & O'Brien, P. J., 2001. Resolving the relationship between high P-T rocks and
581 gneisses in collisional terranes: an example from the Gföhl gneiss-granulite
582 association in the Moldanubian Zone, Austria. *Lithos*, **58**, 33–54.
583 Diener, J. F. A. & Powell, R., 2012. Revised activity-composition models for clinopyroxene
584 and amphibole. *Journal of Metamorphic Geology*, **30**, 131–142.
585 Diener, J. F. A., Powell, R., White, R. W. & Holland, T. J. B., 2007. A new thermodynamic
586 model for clino- and orthoamphiboles in the system Na_2O-CaO-FeO-MgO-Al_2O_3-
587 SiO_2-H_2O-O. *Journal of Metamorphic Geology*, **25**, 631–656.
588 Edel, J. B., Schulmann, K. & Holub, F. V, 2003. Anticlockwise and clockwise rotations of the
589 Eastern Variscides accomodated by dextral lithospheric wrenching: palaeomagnetic
590 and structural evidence. *Journal of the Geological Society*, **160**, 209–218.
591 Faryad, S. W., 2009. The Kutná Hora Complex (Moldanubian zone, Bohemian Massif): A
592 composite of crustal and mantle rocks subducted to HP/UHP conditions. *Lithos*, **109**,
593 193–208.
594 Fiala, J., Matějovská, O. & Vaňková, V., 1987. Moldanubian granulites: source material and
595 petrogenetic considerations. *Neues Jahrbuch für Mineralogie, Abhandlungen*, **157**,
596 133–165.
597 Franěk, J., Schulmann, K. & Lexa, O., 2006. Kinematic and rheological model of exhumation
598 of high pressure granulites in the Variscan orogenic root: example of the Blanský les
599 granulite, Bohemian Massif, Czech Republic. *Mineralogy and Petrology*, **86**, 253–
600 276.
601 Franěk, J., Schulmann, K., Lexa, O., Ulrich, S., Štípská, P., Haloda, J. & Týcová, P., 2011a.
602 Origin of felsic granulite microstructure by heterogeneous decomposition of alkali
603 feldspar and extreme weakening of orogenic lower crust during the Variscan orogeny.
604 *Journal of Metamorphic Geology*, **29**, 103–130.
605 Franěk, J., Schulmann, K., Lexa, O., Tomek, C. & Edel, J. B., 2011b. Model of syn-
606 convergent extrusion of orogenic lower crust in the core of the Variscan belt:
607 implications for exhumation of high-pressure rocks in large hot orogens. *Journal of*
608 *Metamorphic Geology*, **29**, 53–78.
609 Franke, W., 2000. The mid-European segment of the Variscides: tectonostratigraphic units,
610 terrane boundaries and kinematic evolution. In: *Orogenic Processes: Quantification*
611 *and Modelling in the Variscan Belt, Special Publications, 179* (eds Franke, W., Haak,
612 V., Oncken, O. & Tanner, D.), pp. 35–63. The Geological Society of London, London.

613 Friedl, G., Cooke, R. A., Finger, F., McNaughton, N. J. & Fletcher, I. R., 2011. Timing of
614 Variscan HP-HT metamorphism in the Moldanubian Zone of the Bohemian Massif:
615 U-Pb SHRIMP dating on multiply zoned zircons from a granulite from the
616 Dunkelsteiner Wald Massif, Lower Austria. *Mineralogy and Petrology*, **102**, 63–75.
617 Green, E., Holland, T. J. B. & Powell, R., 2007. An order-disorder model for omphacitic
618 pyroxenes in the system jadeite-diopside-hedenbergite-acmite, with applications to
619 eclogitic rocks. *American Mineralogist*, **92**, 1181–1189.
620 Hasalová, P., Janoušek, V., Schulmann, K., Štípská, P. & Erban, V., 2008a. From orthogneiss
621 to migmatite: Geochemical assessment of the melt infiltration model in the Gföhl Unit
622 (Moldanubian Zone, Bohemian Massif). *Lithos*, **102**, 508–537.
623 Hasalová, P., Schulmann, K., Lexa, O., Štípská, P., Hrouda, F., Ulrich, S., Haloda, J. &
624 Týcová, P., 2008b. Origin of migmatites by deformation-enhanced melt infiltration of
625 orthogneiss: a new model based on quantitative microstructural analysis. *Journal of*
626 *Metamorphic Geology*, **26**, 29–53.
627 Hasalová, P., Štípská, P., Powell, R., Schulmann, K., Janoušek, V. & Lexa, O., 2008c.
628 Transforming mylonitic metagranite by open-system interactions during melt flow.
629 *Journal of Metamorphic Geology*, **26**, 55–80.
630 Holland, T. J. B. & Powell, R., 1998. An internally consistent thermodynamic data set for
631 phases of petrological interest. *Journal of Metamorphic Geology*, **16**, 309–343.
632 Holland, T. J. B. & Powell, R., 2003. Activity-composition relations for phases in petrological
633 calculations: an asymmetric multicomponent formulation. *Contributions to*
634 *Mineralogy and Petrology*, **145**, 492–501.
635 Jamieson, R. A., Unsworth, M. J., Harris, N. B. W., Rosenberg, C. L. & Schulmann, K., 2011.
636 Crustal melting and the flow of mountains. *Elements*, **7**, 253-260.
637 Janoušek, V., Finger, F., Roberts, M., Frýda, J., Pin, C. & Dolejš, D., 2004. Deciphering the
638 petrogenesis of deeply buried granites: whole-rock geochemical constraints on the
639 origin of largely undepleted felsic granulites from the Moldanubian Zone of the
640 Bohemian Massif. *Transactions of the Royal Society of Edinburgh-Earth Sciences*, **95**,
641 141–159.
642 Janoušek, V. & Holub, F. V., 2007. The causal link between HP-HT metamorphism and
643 ultrapotassic magmatism in collisional orogens: case study from the Moldanubian
644 Zone of the Bohemian Massif. *Proceedings of the Geologists Association*, **118**, 75–86.

645 Klápová, H., Konopásek, J. & Schulmann, K., 1998. Eclogites from the Czech part of the
646 Erzgebirge: multi-stage metamorphic and structural evolution. *Journal of the*
647 *Geological Society*, **155**, 567-583.
648 Klemd, R. & Bröcker, M., 1999. Fluid influence on mineral reactions in ultrahigh-pressure
649 granulites: a case study in the Snieznik Mts. (West Sudetes, Poland). *Contributions to*
650 *Mineralogy and Petrology*, **136**, 358–373.
651 Kooijman, E., Smit, M. A., Mezger, K. & Berndt, J., 2012. Trace element systematics in
652 granulite facies rutile: implications for Zr geothermometry and provenance studies.
653 *Journal of Metamorphic Geology*, **30**, 397–412.
654 Kotková, J., O'Brien, P. J. & Ziemann, M. A., 2011. Diamond and coesite discovered in
655 Saxony-type granulite: Solution to the Variscan garnet peridotite enigma. *Geology*, **39**,
656 667–670.
657 Kröner, A., O'Brien, P. J., Nemchin, A. A., Pidgeon, R. T., 2000. Zircon ages for high
658 pressure granulites from South Bohemia, Czech Republic, and their connection to
659 Carboniferous high temperature processes. *Contributions to Mineralogy and*
660 *Petrology*, **138**, 127–142.
661 Kryza, R., Pin, C. & Vielzeuf, D., 1996. High-pressure granulites from the Sudetes (south-
662 west Poland): evidence of crustal subduction and collisional thickening in the Variscan
663 Belt. *Journal of Metamorphic Geology*, **14**, 531–546.
664 Lexa, O., Schulmann, K., Janoušek, V., Štípská, P., Guy, A. & Racek, M., 2011. Heat sources
665 and trigger mechanisms of exhumation of HP granulites in Variscan orogenic root.
666 *Journal of Metamorphic Geology*, **29**, 79–102.
667 Liu, Y. C., Gu, X. F., Li, S. G., Hou, Z. H. & Song, B., 2011. Multistage metamorphic events
668 in granulitized eclogites from the North Dabie complex zone, central China: Evidence
669 from zircon U-Pb age, trace element and mineral inclusion. *Lithos*, **122**, 107-121.
670 Medaris, G., Wang, H., Jelínek, E., Mihaljevič, M. & Jakeš, P., 2005. Characteristics and
671 origins of diverse Variscan peridotites in the Gföhl Nappe, Bohemian Massif, Czech
672 Republic. *Lithos*, **82**, 1–23.
673 Medaris, L. G., Beard, B. L., Johnson, C. M., Valley, J. W., Spicuzza, M. J., Jelínek, E. &
674 Mísař, Z., 1995a. Garnet pyroxenite and eclogite in the Bohemian Massif:
675 geochemical evidence for Variscan recycling of subducted lithosphere. *Geologische*
676 *Rundschau*, **84**, 489–505.

677 Medaris, L. G., Fournelle, J. H., Ghent, E. D., Jelínek, E. & Mísař, Z., 1998. Prograde eclogite
678 in the Gföhl Nappe, Czech Republic: new evidence on Variscan high-pressure
679 metamorphism. *Journal of Metamorphic Geology*, **16**, 563–576.
680 Medaris, L. G., Ghent, E. D., Wang, H. F., Fournelle, J. H. & Jelínek, E., 2006. The Spačice
681 eclogite: constraints on the P-T-t history of the Gföhl granulite terrane, Moldanubian
682 Zone, Bohemian Massif. *Mineralogy and Petrology*, **86**, 203–220.
683 Medaris, L. G., Jelínek, E. & Mísař, Z., 1995b. Czech eclogites: Terrane settings and
684 implications for Variscan tectonic evolution of the Bohemian Massif. *European*
685 *Journal of Mineralogy*, **7**, 7–28.
686 Nahodilová, R., Štípská, P., Powell, R., Košler, J. & Racek, M., 2012. High-Ti muscovite as a
687 prograde relict in high pressure granulites with metamorphic Devonian zircon ages
688 (Běstvina granulite body, Bohemian Massif): Consequences for the relamination
689 model of subducted crust. *Gondwana Research*,
690 http://dx.doi.org/10.1016/j.gr.2012.08.021
691 O'Brien, P. J., 2000. The fundamental Variscan problem: high-temperature metamorphism at
692 different depths and high-pressure metamorphism at different temperatures. In:
693 *Orogenic processes: Quantification and modelling in the Variscan belt. Geological*
694 *Society of London, Special publication, 179* (eds Franke, W., Haak, V., Oncken, O. &
695 Tanner, B.), pp. 369–386. The Geological Society of London, London.
696 O'Brien, P. J., 2008. Challenges in high-pressure granulite metamorphism in the era of
697 pseudosections: reaction textures, compositional zoning and tectonic interpretation
698 with examples from the Bohemian Massif. *Journal of Metamorphic Geology*, **26**, 235–
699 251.
700 O'Brien, P. J. & Rötzler, J., 2003. High-pressure granulites: formation, recovery of peak
701 conditions and implications for tectonics. *Journal of Metamorphic Geology*, **21**, 3–20.
702 Obata, M., Hirajima, T. & Svojtka, M., 2006. Origin of eclogite and garnet pyroxenite from
703 the Moldanubian Zone of the Bohemian Massif, Czech Republic and its implication to
704 other mafic layers embedded in orogenic peridotites. *Mineralogy and Petrology*, **88**,
705 321–340.
706 Pouba, Z., Paděra, K. & Fiala, J., 1985. Omphacite granulite from the NE margin of the
707 Bohemian Massif (Rychleby Mts). *Neues Jahrbuch für Mineralogie, Abhandlungen*,
708 **151**, 29–52.

709 Powell, R., Holland, T. J. B. & Worley, B., 1998. Calculating phase diagrams involving solid
710 solutions via non- linear equations, with examples using THERMOCALC. *Journal of*
711 *Metamorphic Geology*, **16**, 577–588.
712 Prince, C. I., Košler, J., Vance, D. & Gunther, D., 2000. Comparison of laser ablation ICP-
713 MS and isotope dilution REE analyses - implications for Sm-Nd garnet
714 geochronology. *Chemical Geology*, **168**, 255–274.
715 Racek, M., Štípská, P., Pitra, P., Schulmann, K. & Lexa, O., 2006. Metamorphic record of
716 burial and exhumation of orogenic lower and middle crust: a new tectonothermal
717 model for the Drosendorf window (Bohemian Massif, Austria). *Mineralogy and*
718 *Petrology*, **86**, 221–251.
719 Racek, M., Štípská, P. & Powell, R., 2008. Garnet-clinopyroxene intermediate granulites in
720 the St. Leonhard massif of the Bohemian Massif: ultrahigh-temperature
721 metamorphism at high pressure or not? *Journal of Metamorphic Geology*, **26**, 253–
722 271.
723 Rebay, G., Powell, R. & Diener, J. F. A., 2010. Calculated phase equilibria for a MORB
724 composition in a P-T range, 450-650 °C and 18-28 kbar: the stability of eclogite.
725 *Journal of Metamorphic Geology*, **28**, 635–645.
726 Rötzler, J. & Romer, R. L., 2001. P-T-t evolution of ultrahigh-temperature granulites from the
727 Saxon Granulite Massif, Germany. Part I: Petrology. *Journal of Petrology*, **42**, 1995–
728 2013.
729 Rötzler, J., Romer, R. L., Budzinski, H. & Oberhansli, R., 2004. Ultrahigh-temperature high-
730 pressure granulites from Tirschheim, Saxon Granulite Massif, Germany: P-T-t path
731 and geotectonic implications. *European Journal of Mineralogy*, **16**, 917–937.
732 Schmädicke, E., Gose, J. & Will, T. M., 2010. The P-T evolution of ultra high temperature
733 garnet-bearing ultramafic rocks from the Saxonian Granulitgebirge Core Complex,
734 Bohemian Massif. *Journal of Metamorphic Geology*, **28**, 489-508.
735 Schmädicke, E., Okrusch, M. & Schmidt, W., 1992. Eclogite-facies rocks in the Saxonian
736 Erzgebirge, Germany: high pressure metamorphism under contrasting P-T conditions.
737 *Contributions to Mineralogy and Petrology*, **110**, 226-241.
738 Schulmann, K., Kröner, A., Hegner, E., Wendt, I., Konopásek, J., Lexa, O. & Štípská, P.,
739 2005. Chronological constraints on the pre-orogenic history, burial and exhumation of
740 deep-seated rocks along the eastern margin of the Variscan orogen, Bohemian Massif,
741 Czech Republic. *American Journal of Science*, **305**, 407–448.

742 Schulmann, K., Lexa, O., Štípská, P., Racek, M., Tajčmanová, L., Konopásek, J., Edel, J. B.,
743 Peschler, A. & Lehmann, J., 2008. Vertical extrusion and horizontal channel flow of
744 orogenic lower crust: key exhumation mechanisms in large hot orogens? *Journal of*
745 *Metamorphic Geology*, **26**, 273–297.
746 Schulmann, K., Konopásek, J., Janoušek, V., Lexa, O., Lardeaux, J. M., Edel, J. B., Štípská,
747 P. & Ulrich, S., 2009. An Andean type Palaeozoic convergence in the Bohemian
748 Massif. *Comptes Rendus Geoscience*, **341**, 266-286.
749 Sláma, J., Košler, J. & Pedersen, R. B., 2007. Behaviour of zircon in high-grade metamorphic
750 rocks: evidence from Hf isotopes, trace elements and textural studies. *Contributions to*
751 *Mineralogy and Petrology*, **154**, 335–356.
752 Smulikowski, K., 1967. Eclogites of the Śnieznik Mts in the Sudetes. *Geologia Sudetica*, **3**,
753 157–174.
754 Steltenpohl, M. G., Cymerman, Z., Krogh, E. J. & Kunk, M. J., 1993. Exhumation of
755 eclogitized continental basement during Variscan lithospheric delamination and
756 gravitational collapse, Sudety Mountains, Poland. *Geology*, **21**, 1111–1114.
757 Štípská, P., Schulmann, K. & Kröner, A., 2004. Vertical extrusion and middle crustal
758 spreading of omphacite granulite: a model of syn-convergent exhumation (Bohemian
759 Massif, Czech Republic). *Journal of Metamorphic Geology*, **22**, 179–198.
760 Štípská, P. & Powell, R., 2005a. Constraining the P-T path of a MORB-type eclogite using
761 pseudosections, garnet zoning and garnet-clinopyroxene thermometry: an example
762 from the Bohemian Massif. *Journal of Metamorphic Geology*, **23**, 725–743.
763 Štípská, P. & Powell, R., 2005b. Does ternary feldspar constrain the metamorphic conditions
764 of high-grade meta-igneous rocks? Evidence from orthopyroxene granulites,
765 Bohemian Massif. *Journal of Metamorphic Geology*, **23**, 627–647.
766 Štípská, P., Schulmann, K. & Powell, R., 2008. Contrasting metamorphic histories of lenses
767 of high-pressure rocks and host migmatites with a flat orogenic fabric (Bohemian
768 Massif, Czech Republic): a result of tectonic mixing within horizontal crustal flow?
769 *Journal of Metamorphic Geology*, **26**, 623–646.
770 Štípská, P., Powell, R., White, R. W. & Baldwin, J. A., 2010. Using calculated chemical
771 potential relationships to account for coronas around kyanite: an example from the
772 Bohemian Massif. *Journal of Metamorphic Geology*, **28**, 97–116.
773 Štípská, P., Chopin, F., Skrzypek, E., Schulmann, K., Pitra, P., Lexa, O., Martelat, J. E.,
774 Bollinger, C. & Žáčková, E., 2012. The juxtaposition of eclogite and mid-crustal rocks

in the Orlica-Snieznik Dome, Bohemian Massif. *Journal of Metamorphic Geology*, **30**, 213–234.

Štípská, P., Powell, R., Racek, M. & Lexa, O., this issue. Intermediate granulite produced by transformation of eclogite at a felsic granulite contact, in Blanský les, Bohemian Massif. *Journal of Metamorphic Geology*, this issue.

Stöckhert, B., Duyster, J., Trepmann, C. & Massonne, H. J., 2001. Microdiamond daughter crystals precipitated from supercritical COH + silicate fluids included in garnet, Erzgebirge, Germany. *Geology*, **29**, 391-394.

Sun, S. S. & McDonough, W. F., 1989. Chemical and isotopic systematics of oceanic basalts: implications for mantle composition and processes. In: *Magmatism in the ocean basins, Geological Society Special Publication, 42* (eds Saunders A. D. & Norry M. J), 313–345. The Geological Society of London, London.

Tajčmanová, L., Konopásek, J. & Schulmann, K., 2006. Thermal evolution of the orogenic lower crust during exhumation within a thickened Moldanubian root of the Variscan belt of Central Europe. *Journal of Metamorphic Geology*, **24**, 119–134.

Tajčmanová, L., Soejono, I., Konopásek, J., Košler, J. & Klötzli, U., 2010. Structural position of high-pressure felsic to intermediate granulites from NE Moldanubian domain (Bohemian Massif). *Journal of the Geological Society*, **167**, 329–345.

Tajčmanová, L., Podlatchikov, Y., Powell, R., Vrijmoed, H., & Moulas, E., 2014. Grain scale pressure variations and chemical equilibrium in high-grade metamorphic rocks. *Journal of Metamorphic Geology*, **22**, *in press*.

Tomkins, H. S., Powell, R., Ellis, D. J., 2007. The pressure dependence of the zirconium-in-rutile thermometer. *Journal of Metamorphic Geology*, **25**, 703–713.

Watson, E. B., Wark, D. A. & Thomas, J. B., 2006. Crystallization thermometers for zircon and rutile. *Contributions to Mineralogy and Petrology*, **151**, 413–433.

White, R. W., Powell, R., Holland, T. J. B., 2007. Progress relating to calculation of partial melting equilibria for metapelites. *Journal of Metamorphic Geology*, **25**, 511–527.

White, R. W., Powell, R., Holland, T. J. B., Worley, B. A., 2000. The effect of TiO_2 and Fe_2O_3 on metapelitic assemblages at greenschist and amphibolite facies conditions: mineral equilibria calculations in the system K_2O-FeO-MgO-Al_2O_3-SiO_2-H_2O-TiO_2-Fe_2O_3. *Journal of Metamorphic Geology*, **18**, 497–511.

Willner, A. P., Rötzler, K. & Maresch, W. V., 1997. Pressure - Temperature and fluid evolution of quartzo-feldspathic metamorphic rocks with a relic high-pressure,

granulite-facies history from the Central Erzgebirge (Saxony, Germany). *Journal of Petrology*, **38**, 307-336.

Willner, A. P., Krohe, A. & Maresch, W. V., 2000. Interrelated P-T-t-d paths in the Variscan Erzgebirge dome (Saxony, Germany): Constraints on the rapid exhumation of high-pressure rocks from the root zone of a collisional Orogen. *International Geology Review*, **42**, 64-85.

Figure captions

Fig. 1. Geological map of the Bohemian Massif (after Franke, 2000). Location of the study area is indicated. Left inset is position of study area in the framework of the European Variscides (after Edel *et al.*, 2003).

Fig. 2. Field relations of the eclogite studied. (a) Outcrop dominated by dark intermediate granulite with white layers of felsic granulite. (b) At the boundary of a felsic granulite layer with intermediate granulite, cuspate-lobate relationships occur, showing lower viscosity of the felsic granulite. In the internal parts of the lobate forms of the intermediate granulite are bodies of eclogite. (c) Eclogite bodies within the intermediate granulite. (d) Greenish eclogite with dark amphibole-bearing patches and red garnet at boundary with intermediate granulite with macroscopically-visible white feldspar-bearing domains. (e) 0.5 m large eclogite body with relatively sharp boundaries with respect to layered felsic granulite. (f) Detail of eclogite at boundary with intermediate granulite.

Fig. 3. BSE images of eclogite. (a) Garnet within texturally equilibrated matrix. The location of chemical profiles indicated by arrows. (b) Detail of texturally equilibrated matrix. (c) Detail of garnet surrounded by multigrain plagioclase corona. (d) Fine-grained kelyphitic embayments of plagioclase and amphibole in garnet. (e) Fine grained kelyphite replacing garnet. (f) Garnet with left side surrounded mainly by plagioclase corona, and right side surrounded by amphibole-plagioclase dominated kelyphite with minor orthopyroxene. Omphacitic clinopyroxene inclusion in garnet. (g) Detail of fine-grained kelyphite dominated by amphibole and plagioclase, and minor orthopyroxene. Note the larger amphibole and ilmenite in the plagioclase matrix.

Fig. 4. BSE images of inclusions in garnet. (a) Large garnet with omphacite inclusion. (b) Detail of omphacite inclusion with idiomorphic shapes. (c) Inclusions of zircon and rutile. (d) Large garnet with omphacite inclusion. (e) Detail of idiomorphic omphacite, chemical profile is indicated. (f) Inclusion of idiomorphic quartz. (g) Rim area of large garnet contains

inclusions of omphacite and plagioclase. (h) Detail of plagioclase inclusion shows idiomorphic shape. (i) Detail of clinopyroxene inclusion.

Fig. 5. Calculated proportions of (a) garnet (11%) and (b) garnet with plagioclase corona and plagioclase-amphibole kelyphite (33%).

Fig. 6. Compositional maps of garnet and surrounding areas. For detail see text.

Fig. 7. Composition and zoning of minerals in textural positions as indicated.

Fig. 8. Zr content in rutile and temperature from the Zr-in-rutile thermometer of Tomkins *et al.* (2007). The results are presented in the form of box-plots. In a box-plot, the box is given by the interquartile range of the data (the middle half of the data), the line across the box is at the median of the data, and the whiskers extend out to the furthest datapoint that is within 1.5 times the interquartile range from the box. Dots are points beyond the whiskers (outliers). The number of analyses is marked.

Fig. 9. $P-T$ pseudosection calculated for the rock composition of the eclogite sample KL1i (a). The ellipses indicate areas of $P-T$ equilibration derived by comparing the modelled assemblages and isopleths with assemblages, chemistry and zoning of minerals observed in the sample. (b,c,e) The pseudosection with calculated isopleths of molar proportions and mineral composition.

Fig. 10. Dry $P-X$ pseudosection varying the proportion of garnet included in the bulk composition, showing its control on the matrix phase relationships. For details see text.

Fig. 11. H_2O-undersaturated pseudosection for the eclogite sample KL1i. The ellipses indicate areas of $P-T$ equilibration. For details see text.

Fig. 12. $T-M(H_2O)$ and $T-\mu(H_2O)$ diagrams contoured with molar proportion of amphibole are used for discussion of significance of coarse-grained amphibole in the equilibrated matrix and formation of fine-grained amphibole-plagioclase kelyphite. For details see text.

Fig. 13. Summarization of microstructural evolution of the eclogite along the inferred $P-T$ path. Microstructural changes related to changes in $P-T$ conditions are in white circles.

Table 1. Representative mineral analyses of garnet and amphibole. Mx=matrix, in=inclusion, kel=kelyphite, r=rim, c-core, cont-contact.

Table 2. Representative mineral analyses of clinopyroxene and orthopyroxene. Mx=matrix, in=inclusion, kel=kelyphite, r=rim, c-core.

Table 3. Representative mineral analyses of plagioclase. Mx=matrix, in=inclusion, cor=corona, kel=kelyphite, r=rim, c-core, +g=at contact with garnet.

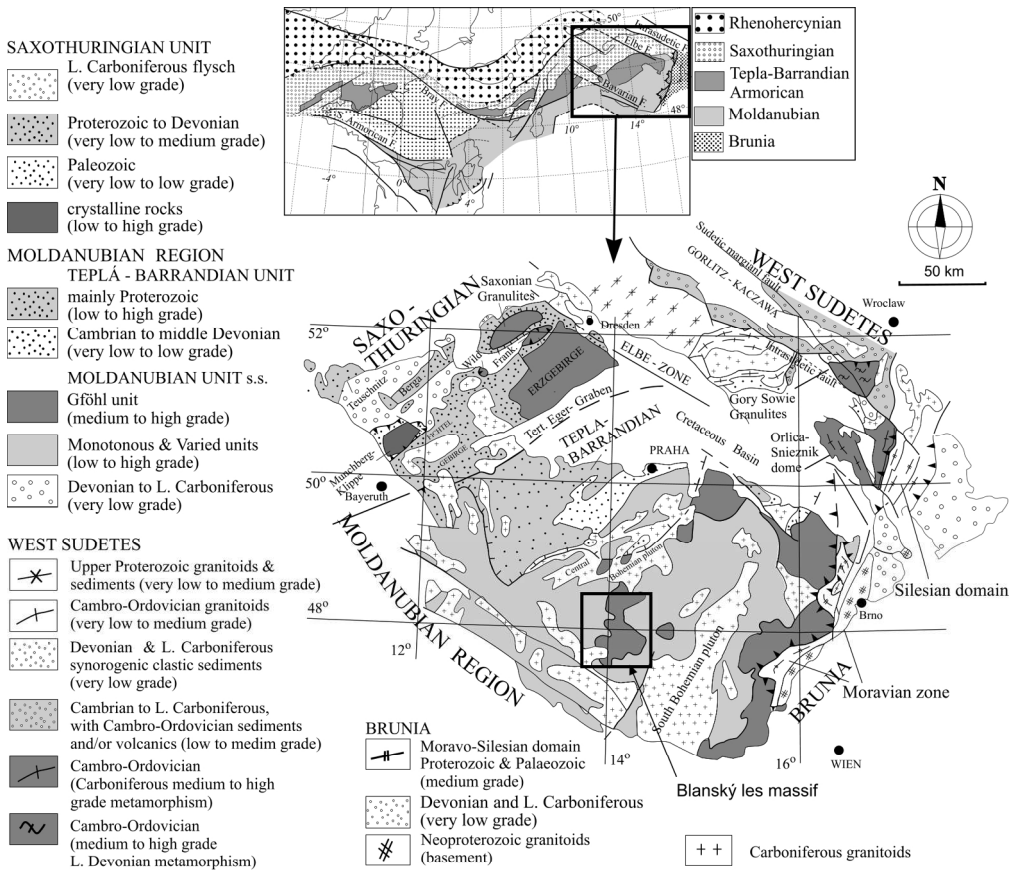

F01-Bohmasmap

164x158mm (300 x 300 DPI)

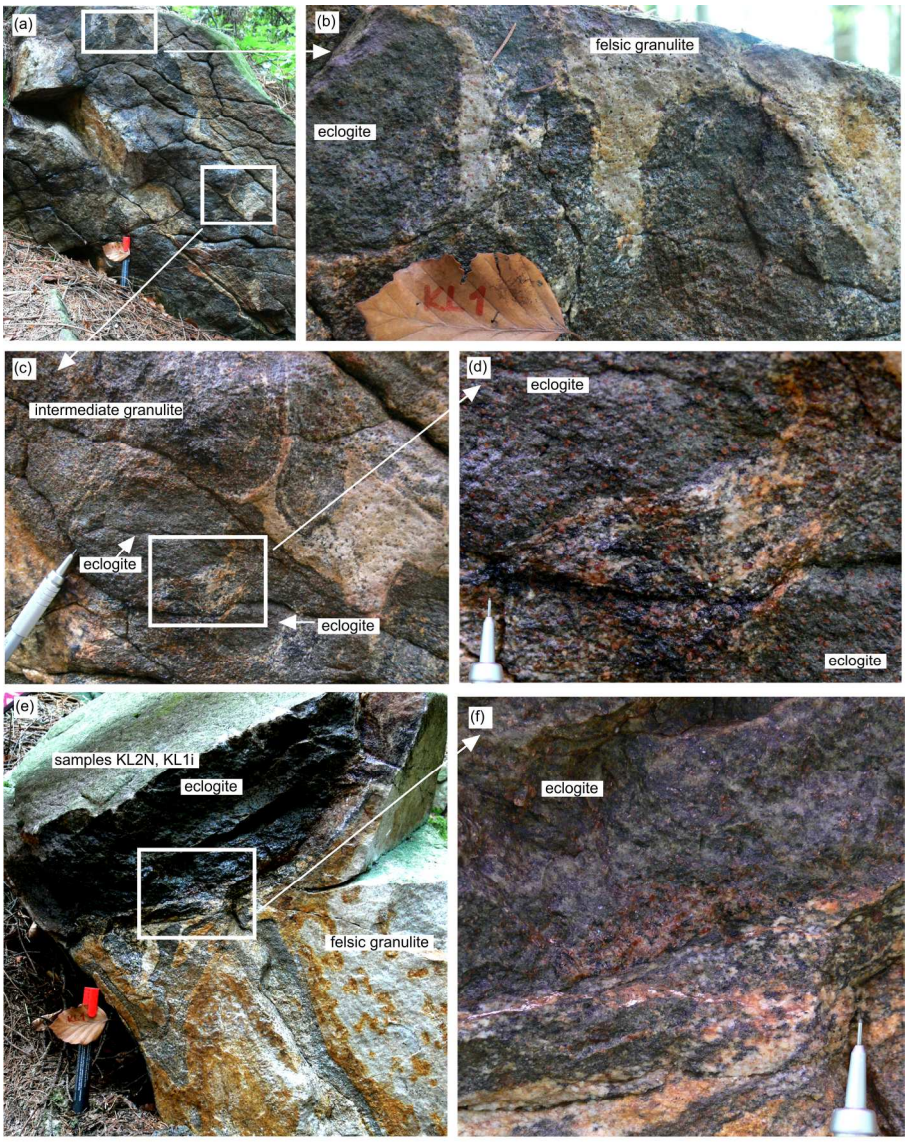

Fig. 02 [fieldphotos]

165x219mm (300 x 300 DPI)

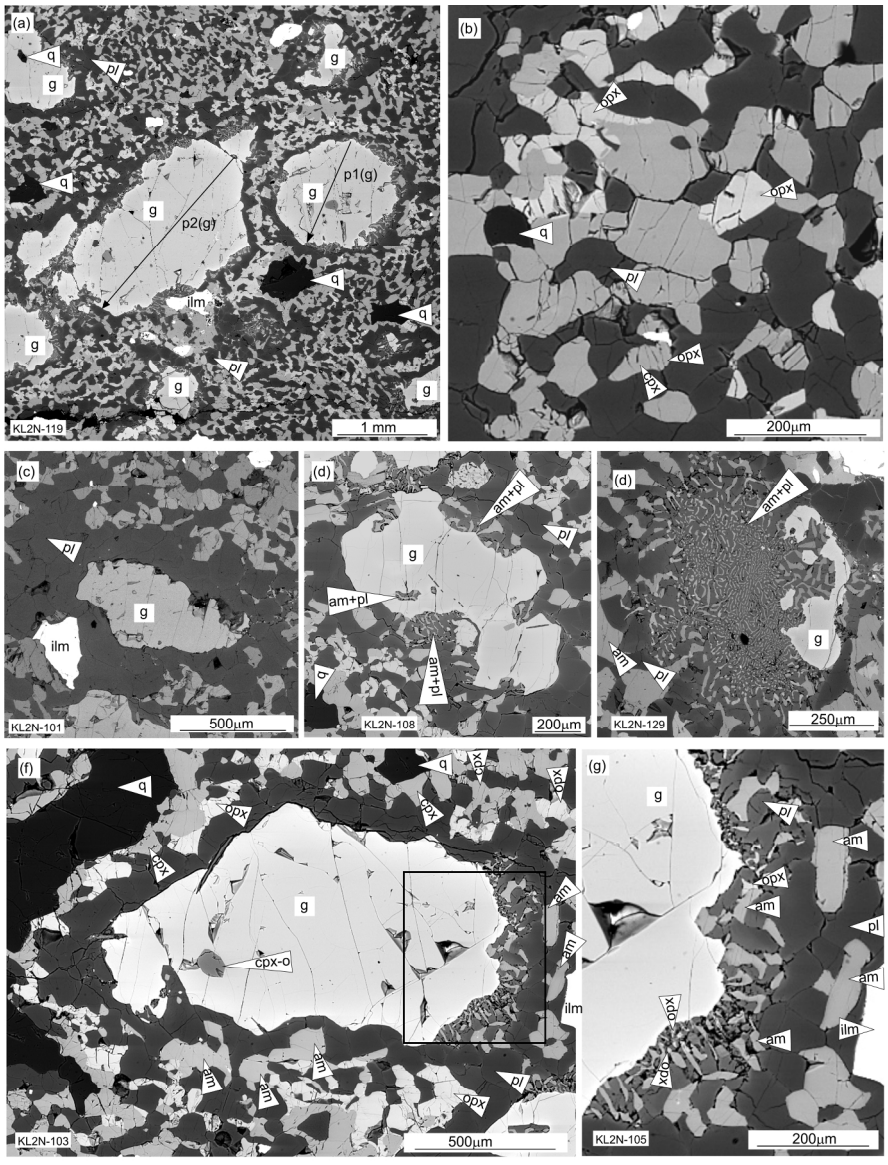

Fig. 03 [photo-micro1]

172x235mm (300 x 300 DPI)

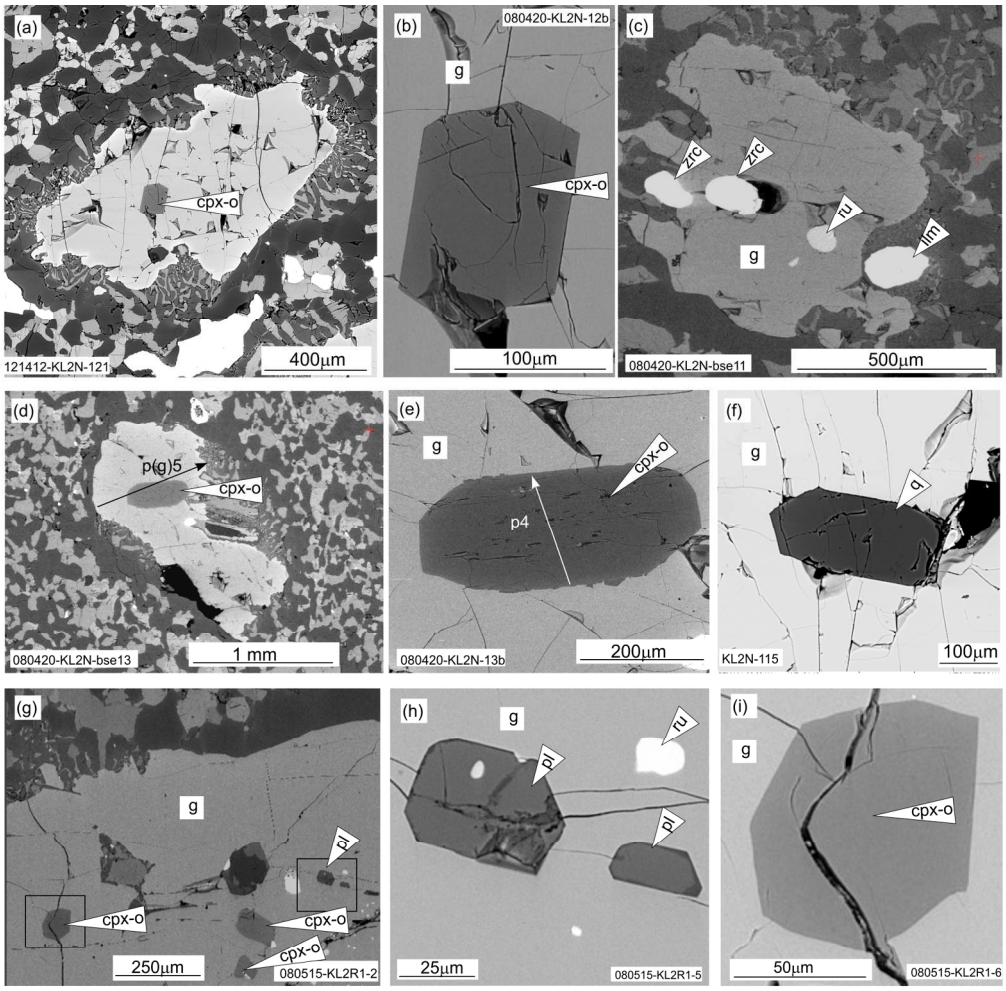

F04 [photo-inclusions]

165x190mm (300 x 300 DPI)

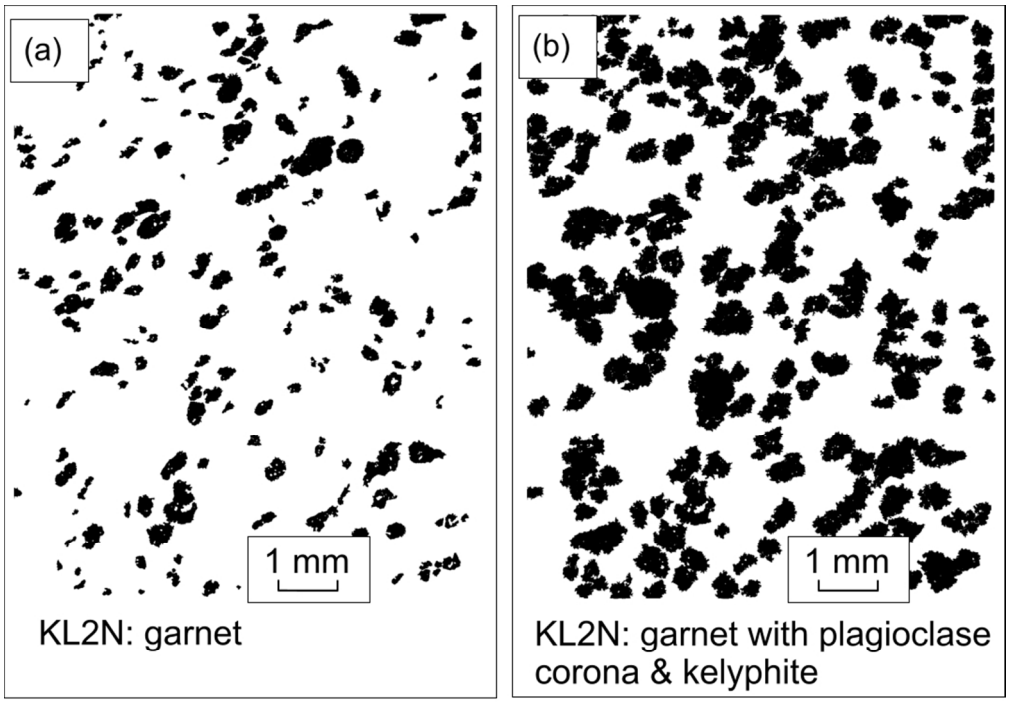

Fig. 05 [modegrt]

90x77mm (300 x 300 DPI)

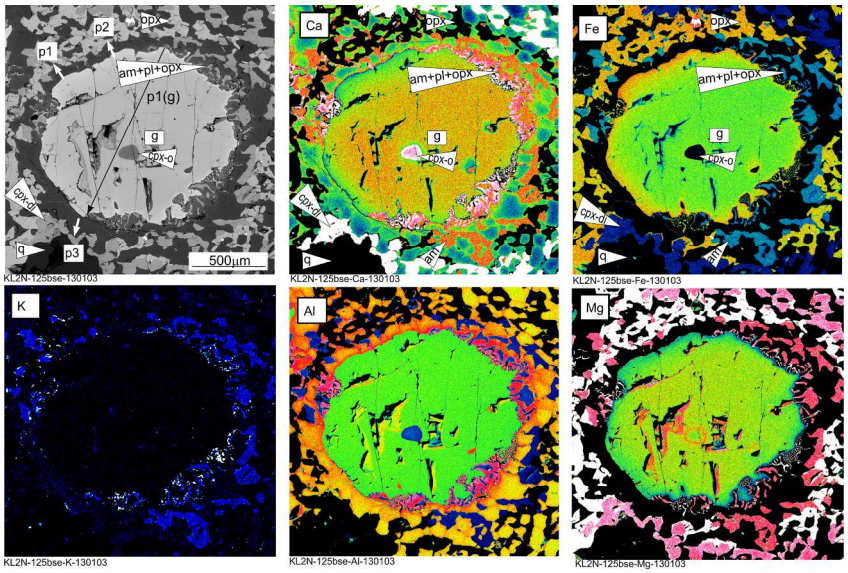

Fig. 06 [element-maps]

184x264mm (300 x 300 DPI)

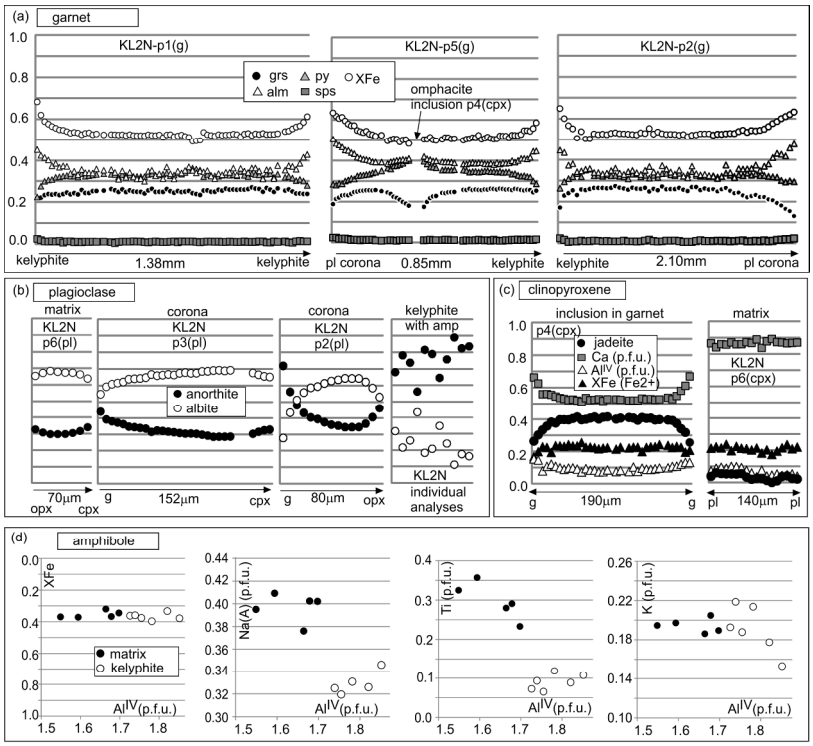

Fig. 07 [chemistry]

169x252mm (300 x 300 DPI)

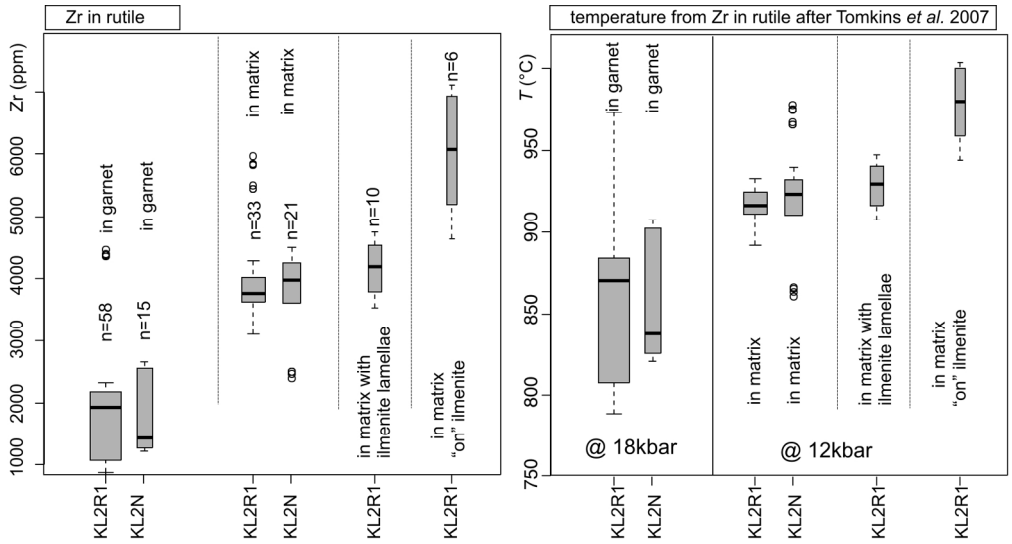

Fig. 08 [rutile]

158x119mm (300 x 300 DPI)

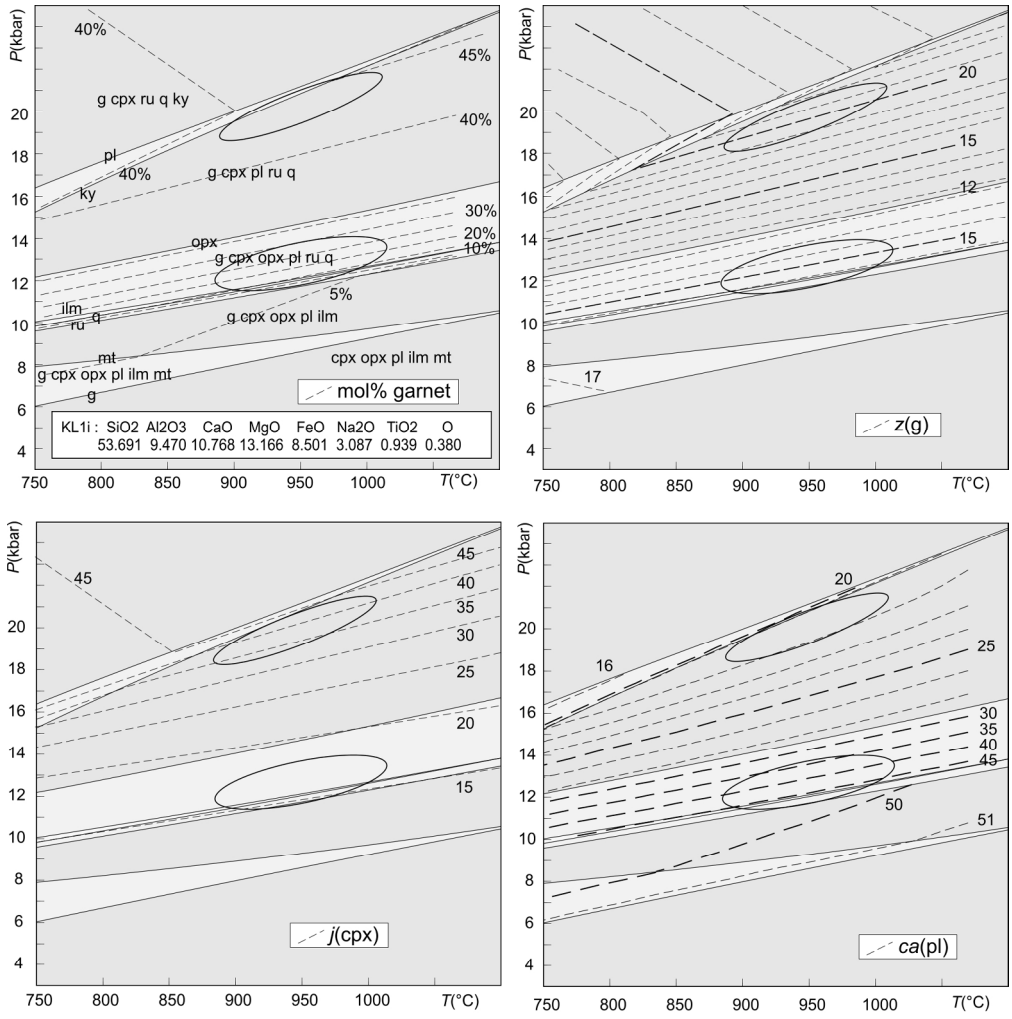

Fig. 09 [drypseu]

174x185mm (300 x 300 DPI)

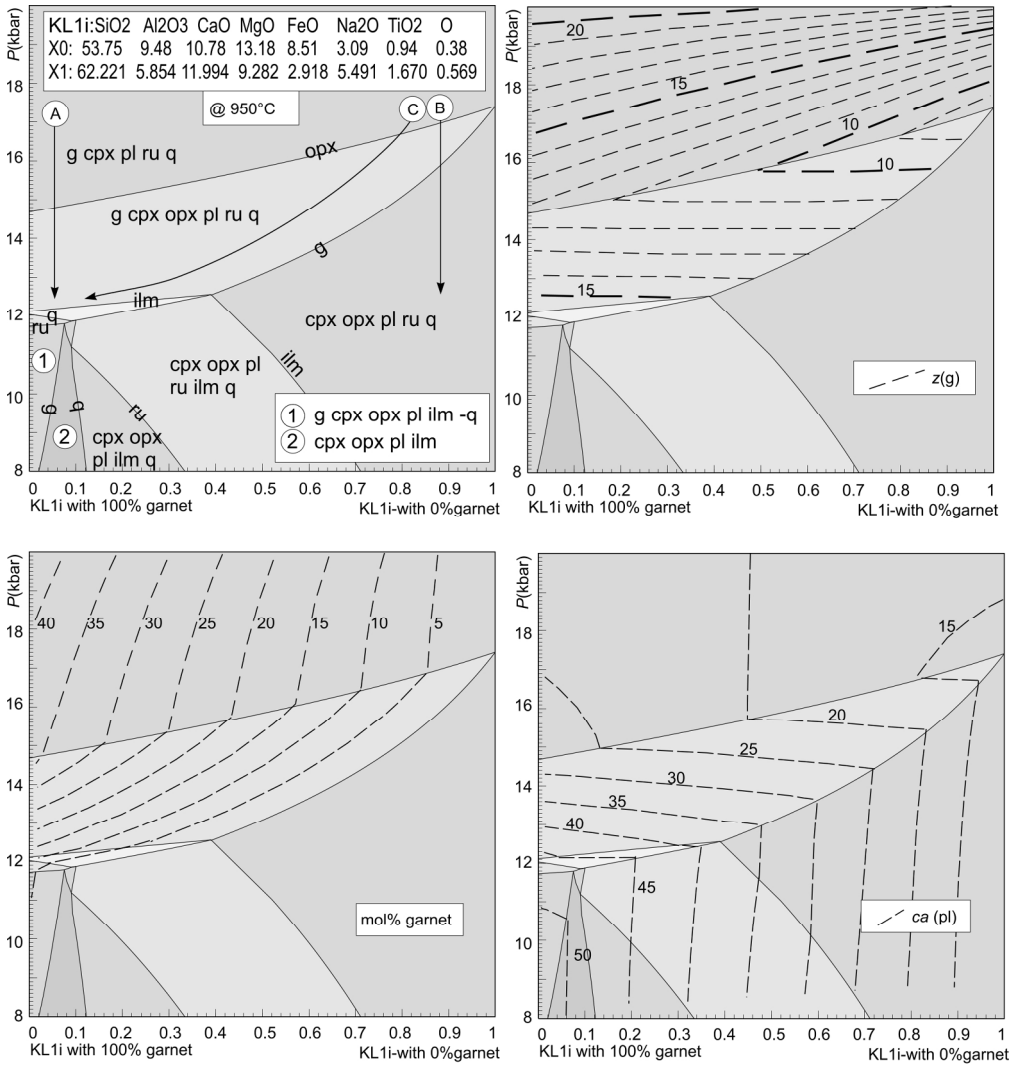

Fig. 10 [PX]

174x195mm (300 x 300 DPI)

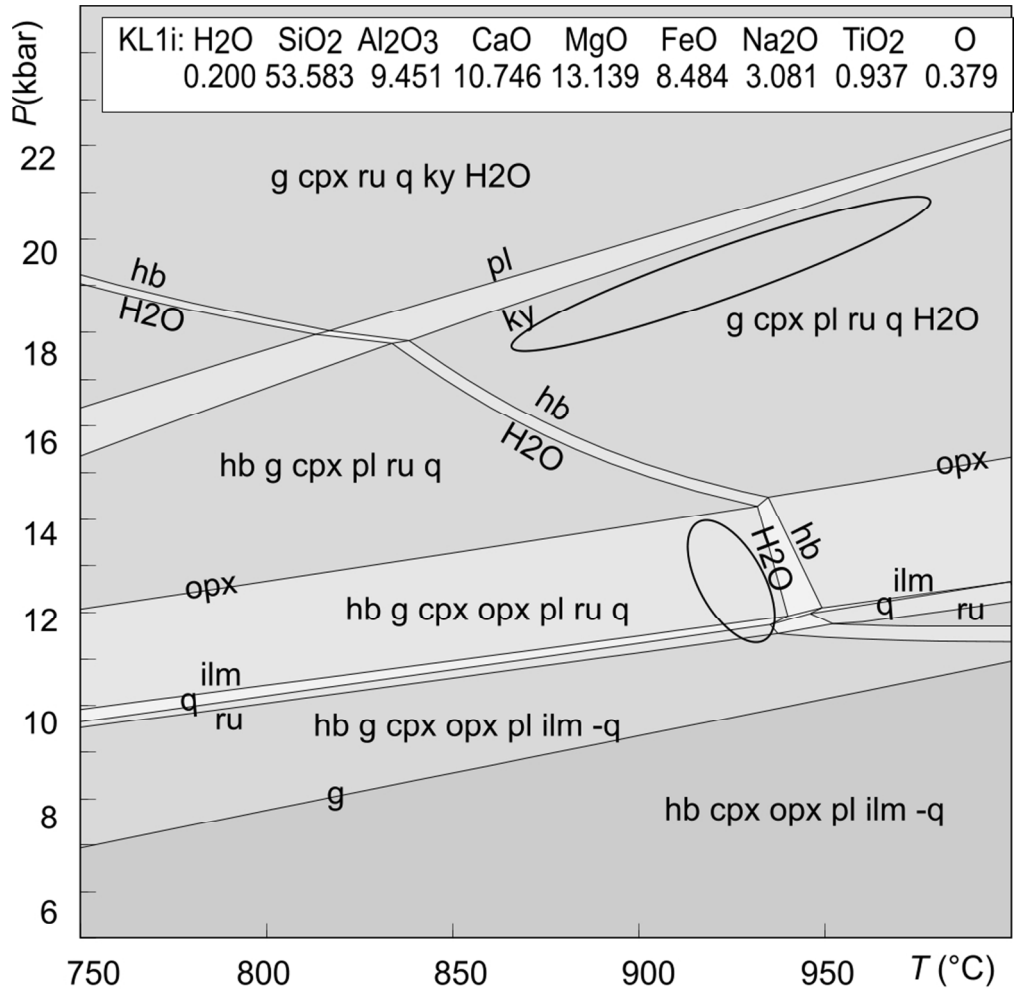

Fig. 11 [H2O-pseu]

90x101mm (300 x 300 DPI)

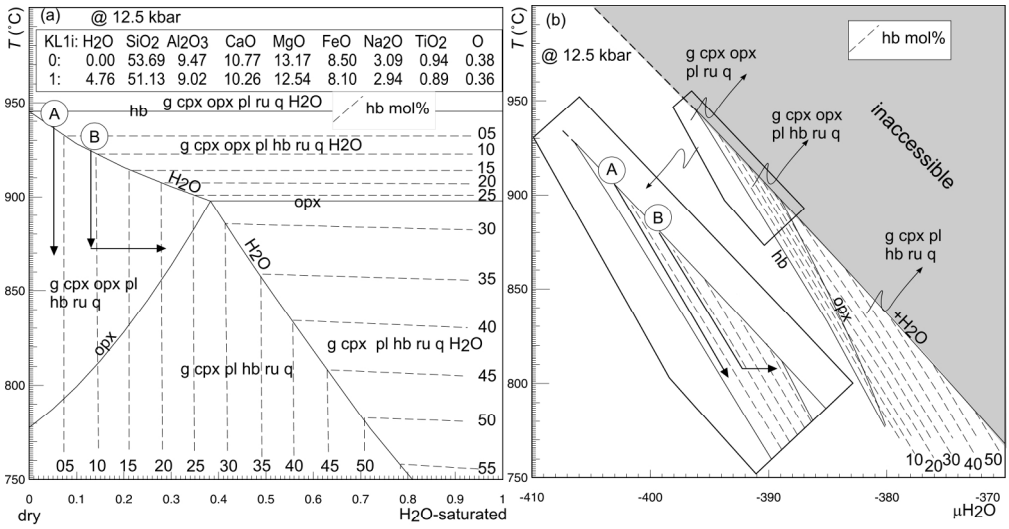

Fig.12 [T-H2O]

171x105mm (300 x 300 DPI)

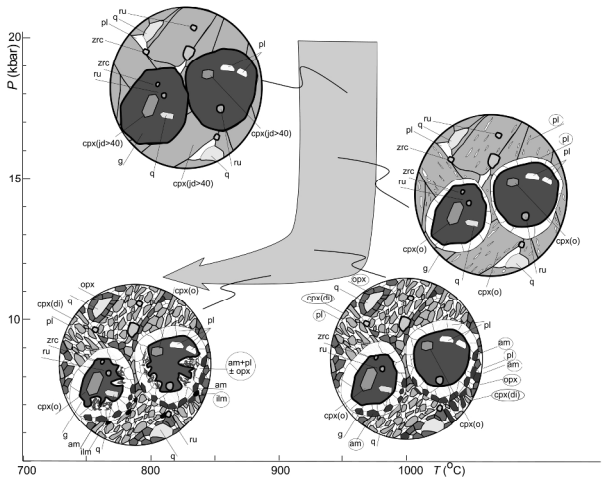

Fig 13 [mineral comix]

210x297mm (300 x 300 DPI)

Table 1. Representative mineral analyses of garnet and amphibole
Mx=matrix, in=inclusion, kel=kelyphite, r=rim, c-core, cont-contact.

Sample	KL2N	KL2N	KL2N	KL2N	KL2N	KL2N	KL2N	KL2N	KL2N
Mineral	g	g	g	g	g	g	g	am	am
Position	c	c	mx-r	mx-r	kel-r	kel-r	cont+omphacite	mx	kel
Spectrum	S28	S29	S2	S64	S23	S89	S19	S4	2-am
SiO_2	39.76	40.04	38.77	38.73	38.80	38.46	39.39	44.04	42.87
TiO_2	0.13	0.09	0.00	0.09	0.16	0.21	0.00	2.95	1.09
Cr_2O_3	0.12	0.00	0.00	0.08	0.05	0.00	0.00	0.27	0.17
Al_2O_3	22.47	22.46	22.00	21.88	21.88	21.81	22.37	9.95	12.99
FeO	17.64	17.66	23.61	22.70	21.27	22.53	19.56	11.25	12.44
MnO	0.40	0.34	0.99	0.92	0.76	0.93	0.38	0.14	0.16
MgO	9.12	9.13	7.95	7.50	6.98	6.58	10.35	12.97	13.02
CaO	10.64	10.77	6.59	7.54	9.56	8.98	7.11	11.66	11.37
Na_2O	0.00	0.00	0.00	0.00	0.00	0.00	0.00	1.59	1.88
K_2O	0.00	0.00	0.00	0.00	0.00	0.00	0.00	0.78	0.82
Total	100.28	100.48	99.92	99.43	99.46	99.50	99.16	95.60	96.81
Si	2.99	3.00	2.98	2.99	2.99	2.98	2.99	6.58	6.26
Ti	0.01	0.00	0.00	0.01	0.01	0.01	0.00	0.33	0.12
Cr	0.01	0.00	0.00	0.00	0.00	0.00	0.00	0.03	0.02
Al	1.99	1.98	1.99	1.99	1.99	1.99	2.00	1.75	2.24
Fe^{3+}	0.02	0.01	0.06	0.02	0.01	0.03	0.02	0.06	0.76
Fe^{2+}	1.09	1.10	1.46	1.45	1.36	1.42	1.22	1.34	0.76
Mn	0.03	0.02	0.06	0.06	0.05	0.06	0.02	0.02	0.02
Mg	1.02	1.02	0.91	0.86	0.80	0.76	1.17	2.89	2.83
Ca	0.86	0.86	0.54	0.62	0.79	0.74	0.58	1.87	1.78
Na	0.00	0.00	0.00	0.00	0.00	0.00	0.00	0.46	0.53
K	0.00	0.00	0.00	0.00	0.00	0.00	0.00	0.15	0.15
Total	8.00	8.00	8.00	8.00	8.00	8.00	8.00	15.47	15.46
XFe	0.52	0.52	0.62	0.63	0.63	0.65	0.51	0.32	0.21
alm/NaA	0.36	0.37	0.49	0.48	0.45	0.48	0.41	0.33	0.31
py/NaM4	0.34	0.34	0.31	0.29	0.27	0.25	0.39	0.13	0.22
grs	0.29	0.29	0.18	0.21	0.26	0.25	0.19		
sps	0.01	0.01	0.02	0.02	0.02	0.02	0.01		

Table 2. Representative mineral analyses of clinopyroxene and orthopyroxene
Mx=matrix, in=inclusion, kel=kelyphite, r=rim, c-core.

Sample	KL2N	KL2N	KL2N	KL2N	KL2N	KL2N	KL2N	KL2N	KL2N
Mineral	cpx	cpx	cpx	cpx	cpx	cpx	opx	opx	opx
Position	in-c	in-c	in-r	in-r	mx	mx	mx	mx	kel
Spectrum	S14	S15	S8	S18	S6	S11	S12	S13	3-opx
SiO_2	54.21	54.28	52.17	51.98	52.02	51.32	52.12	52.08	52.05
TiO_2	0.29	0.27	0.65	0.82	0.37	0.50	0.12	0.08	0.08
Cr_2O_3	0.02	0.05	0.00	0.06	0.10	0.11	0.12	0.04	0.15
Al_2O_3	13.23	13.23	11.80	10.74	2.57	3.30	1.04	0.93	1.97
FeO	4.12	4.31	4.47	4.62	8.28	8.80	22.96	23.15	22.07
MnO	0.00	0.00	0.00	0.00	0.20	0.06	0.33	0.34	0.40
MgO	8.41	8.27	9.84	10.71	13.27	13.38	20.95	20.93	21.65
CaO	14.19	13.86	17.01	17.97	21.92	21.16	0.59	0.61	0.43
Na_2O	5.73	5.83	4.04	3.43	0.47	0.52	0.00	0.00	0.00
K_2O	0.00	0.00	0.00	0.00	0.00	0.00	0.00	0.00	0.00
Total	100.21	100.12	99.97	100.34	99.20	99.16	98.24	98.17	98.79
Si	1.93	1.93	1.88	1.87	1.95	1.92	1.99	1.99	1.96
Ti	0.01	0.01	0.02	0.02	0.01	0.01	0.00	0.00	0.00
Cr	0.00	0.00	0.00	0.00	0.00	0.00	0.00	0.00	0.00
Al	0.56	0.56	0.50	0.46	0.11	0.15	0.05	0.04	0.09
Fe^{3+}	0.00	0.00	0.00	0.00	0.00	0.01	0.00	0.00	0.00
Fe^{2+}	0.12	0.13	0.13	0.14	0.26	0.26	0.73	0.74	0.70
Mn	0.00	0.00	0.00	0.00	0.01	0.00	0.01	0.01	0.01
Mg	0.45	0.44	0.53	0.58	0.74	0.75	1.19	1.19	1.22
Ca	0.54	0.53	0.66	0.69	0.88	0.85	0.02	0.03	0.02
Na	0.40	0.40	0.28	0.24	0.03	0.04	0.00	0.00	0.00
K	0.00	0.00	0.00	0.00	0.00	0.00	0.00	0.00	0.00
Total	4.00	4.00	4.00	4.00	4.00	4.00	4.00	4.00	4.00
Al^{IV}	0.07	0.07	0.12	0.13	0.05	0.08	0.01	0.01	0.04
XFe	0.22	0.23	0.20	0.19	0.26	0.26	0.38	0.38	0.36
jd	0.40	0.40	0.28	0.24	0.03	0.04			

Table 3. Representative mineral analyses of plagioclase.
Mx=matrix, in=inclusion, cor=corona, kel=kelyphite, r=rim, c-core, +g=at contact with garnet.

Sample	KL2N	KL2N	KL2N	KL2N	KL2N	KL2N	KL2N	KL2N	KL2N	KL2N	KL2N
Mineral	pl	pl	pl	pl	pl	pl	pl	pl	pl	pl	pl
Position	in-c	in-r	in-c	mx-c	mx-c	mx-r	mx-r	cor-c	cor+g	cor+cpx	kel.
Spectrum	S18	S17	15-pl	S2	S9	S3	S10	S60	S58	S61	13-pl
SiO_2	60.93	59.19	55.39	59.97	62.51	58.93	59.91	61.21	57.56	60.53	45.45
TiO_2	0.00	0.00	0.00	0.00	0.00	0.00	0.00	0.00	0.00	0.00	0.00
Cr_2O_3	0.00	0.00	0.00	0.00	0.00	0.00	0.00	0.00	0.00	0.00	0.00
Al_2O_3	25.09	26.05	27.79	25.60	24.03	27.03	25.82	24.81	27.45	25.45	35.04
FeO	0.19	0.25	0.45	0.15	0.15	0.27	0.18	0.16	0.25	0.15	0.18
MnO	0.00	0.00	0.00	0.00	0.00	0.00	0.00	0.00	0.00	0.00	0.00
MgO	0.00	0.00	0.00	0.00	0.00	0.00	0.00	0.00	0.00	0.00	0.00
CaO	6.42	7.57	9.93	6.97	5.21	8.24	7.15	6.18	8.99	6.74	17.80
Na_2O	7.60	6.93	5.75	7.52	8.36	7.06	7.58	8.02	6.65	7.76	1.47
K_2O	0.86	0.70	0.16	0.31	0.50	0.26	0.38	0.42	0.18	0.29	0.03
Total	101.09	100.68	99.47	100.52	100.75	101.80	101.03	100.80	101.08	100.91	99.96
Si	2.69	2.63	2.51	2.66	2.76	2.59	2.64	2.70	2.55	2.67	2.09
Ti	0.00	0.00	0.00	0.00	0.00	0.00	0.00	0.00	0.00	0.00	0.00
Cr	0.00	0.00	0.00	0.00	0.00	0.00	0.00	0.00	0.00	0.00	0.00
Al	1.30	1.36	1.48	1.34	1.25	1.40	1.34	1.29	1.43	1.32	1.90
Fe	0.01	0.01	0.02	0.01	0.01	0.01	0.01	0.01	0.01	0.01	0.01
Mn	0.00	0.00	0.00	0.00	0.00	0.00	0.00	0.00	0.00	0.00	0.00
Mg	0.00	0.00	0.00	0.00	0.00	0.00	0.00	0.00	0.00	0.00	0.00
Ca	0.30	0.36	0.48	0.33	0.25	0.39	0.34	0.29	0.43	0.32	0.88
Na	0.65	0.60	0.50	0.65	0.71	0.60	0.65	0.69	0.57	0.66	0.13
K	0.05	0.04	0.01	0.02	0.03	0.01	0.02	0.02	0.01	0.02	0.00
Total	5.00	5.00	5.00	5.00	5.00	5.00	5.00	5.00	5.00	5.00	5.00
an	0.30	0.36	0.48	0.33	0.25	0.39	0.34	0.29	0.42	0.32	0.87
ab	0.65	0.60	0.51	0.65	0.72	0.60	0.64	0.68	0.57	0.66	0.13
or	0.05	0.04	0.01	0.02	0.03	0.01	0.02	0.02	0.01	0.02	0.00